

# Models, Methods and Waveforms for Estimation and Prediction of Doubly Sparse Time-Varying Channels

Wissal Benzine<sup>1,2</sup>, Ali Bemani<sup>1</sup>, Nassar Ksairi<sup>1</sup>, and Dirk Slock<sup>2</sup>

<sup>1</sup>Mathematical and Algorithmic Sciences Lab, Huawei France R&D, Paris, France

<sup>2</sup>Communication Systems Department, EURECOM, Sophia Antipolis, France

Emails: {Wissal.Benzine, Dirk.Slock}@eurecom.fr, {ali.bemani,  
nassar.ksairi}@huawei.com

## Abstract

This paper investigates channel estimation for linear time-varying (LTV) wireless channels under *double sparsity*, i.e., sparsity in both the delay and Doppler domains. An on-grid approximation is first considered, enabling rigorous hierarchical-sparsity modeling and compressed sensing-based channel estimation. Guaranteed recovery conditions are provided for affine frequency division multiplexing (AFDM), orthogonal frequency division multiplexing (OFDM) and single-carrier modulation (SCM), highlighting the superiority of AFDM in terms of doubly sparse channel estimation. To address arbitrary Doppler shifts, a relaxed version of the on-grid model is introduced by making use of multiple elementary Expansion Models (BEM) each based on Discrete Prolate Spheroidal Sequences (DPSS). Next, theoretical guarantees are provided for the precision of this off-grid model before further extending it to tackle channel prediction by exploiting the inherent DPSS extrapolation capability. Finally, numerical results are provided to both validate the proposed off-grid model for channel estimation and prediction purposes under the double sparsity assumption and to compare the corresponding mean squared error (MSE) and the overhead performance when the different wireless waveforms are used.

## Index Terms

channel estimation, time-varying channels, AFDM, sparsity, basis expansion model, Slepian basis, DPSS, channel prediction

## I. INTRODUCTION

Sparsity is an important feature of wireless channels, particularly in high-frequency bands. Sparsity emerges due to the limited number of dominant scatterers contributing to signal propagation and manifests both in the delay and the Doppler domains. By leveraging sparsity, advanced estimation methods can mitigate the challenges posed on channel estimation and prediction by high-mobility scenarios. The question thus arises as to 1) what delay-Doppler modeling can best leverage sparsity to enable efficient and low-complexity estimation and prediction of time-varying channels and 2) which wireless waveforms can make the best use of delay-Doppler sparsity e.g., for pilot overhead reduction.

In wireless communication systems operating in sub-6GHz frequency bands, sparsity is often observed in the delay domain, where only a few dominant delay taps carry most of the channel energy [1]. Channel estimation methods leveraging this delay-domain sparsity have been proposed in various studies, such as [2] in which a grid-based discretization of the delay dimension is used to enable a compressive sensing framework. However, in higher-frequency bands, sparsity extends to the Doppler domain as well in scenarios such as vehicular or high-speed train communications. Delay-Doppler sparsity was assumed in [3] and leveraged to conceive enhanced channel estimation schemes for time-varying channels. However, sparsity was modeled as the sparsity of a one-dimensional array with no way to assign different sparsity levels to the delay and Doppler domains. The model in [4] also assumes a form of delay-Doppler sparsity, though under the restrictive assumption of one Doppler shift per delay tap. On-grid models, assuming that delay and Doppler shifts are quantized to a predefined grid, allow for structured sparse recovery methods. This quantization simplifies estimation but introduces grid mismatch errors [5]. To overcome the limitations of strict grid-based models, off-grid channel estimation techniques have been introduced by relaxing the assumption of discretized delay or Doppler shifts. Having estimates of the fractional part of Doppler frequency shifts enables straightforward channel extrapolation and, hence, prediction. Grid refinement techniques [6], [7] have been explored as a simple and low-complexity method to mitigate the performance degradation caused by grid mismatches. More advanced gridless approaches offering super-resolution recovery have also been investigated [3], [8]–[10]. Off-grid sparse Bayesian learning (SBL) [3], [9] is one such solution. Another solution based on atomic norm minimization is proposed in [10]. Such approaches can offer in principle better performance than grid refinement solutions but at the

cost of higher computational complexity. Moreover, they cannot fully eliminate basis mismatch between real-world signals and the grid, leading to residual errors. They could also suffer from ill conditioning. This is particularly the case, as is argued in Sections IV and V, when the propagation link is characterized by a large number of “physical” channel paths contributing to each of the (refined) grid points. As an alternative, basis expansion models (BEM) can in principle be made to exploit sparsity. For example, the BEM based methods in [11]–[13] take advantage of sparsity, though only in the delay domain. There is thus a need to add support for Doppler domain sparsity to the BEM approach.

Concerning waveforms conceived to deal with high-mobility scenarios, orthogonal time frequency space (OTFS) uses a two-dimensional (2D) modulation technique that transmits the information and pilot symbols in the delay-Doppler domain [14]. However, channel estimation overhead in OTFS cannot be reduced when the channel exhibits sparsity. Indeed, the performance gap between OTFS and OFDM narrows in favor of OFDM on channels with delay domain sparsity [14]. Another recently proposed waveform for communications in high-mobility scenarios is Affine Frequency Division Multiplexing (AFDM) [15]. While in AFDM data and pilot symbols are not directly transmitted in the delay-Doppler domain, AFDM can still reconstruct a delay-Doppler representation of the channel achieving full diversity on doubly dispersive channels. In the absence of sparsity, this leads to AFDM having a comparable bit error rate (BER) performance to that of OTFS but with the advantage of requiring less channel estimation overhead [15]. Under sparsity, our previous works [16], [17] proved the superiority of AFDM over both OFDM and OTFS in terms of pilot overhead using an on-grid channel model. In the current work, we build on those works and on a new sparsity modeling paradigm to expand our results to time-varying channel with off-grid Doppler frequency shifts and we include the study of channel prediction as a key application of this extension.

### *Contributions*

- 1) The statistical notion of delay-Doppler double sparsity (DS) for LTV channels is defined and rigorously linked to the hierarchical sparsity paradigm under a first on-grid approximation of Doppler shifts. This link is used to propose a sparse recovery algorithm for delay-Doppler profiles of wireless channels. Using hierarchical-sparsity mathematical tools, closed-form asymptotic results for the performance of this recovery is provided.

- 2) The effect of the waveform in use on DS-LTV channel estimation is analyzed using these theoretical results pointing to the superiority of AFDM over recovery schemes based on other waveforms in terms of channel estimation overhead.
- 3) A relaxation of the on-grid model to allow for off-grid Doppler frequency shifts is provided, resulting in a novel representation for LTV channels based on multiple elementary BEMs.
- 4) A new theoretical result is derived showing a logarithmic dependency in the inverse of the target mean-square error of the number of DPSS basis vectors needed to guarantee that target error when representing a samples vector from a narrow-band signal occupying a unit-frequency resolution bandwidth in the limit of large samples vector length. Such a signal is relevant because the channel component associated with a cluster of propagation paths sharing the same delay-Doppler grid point can modeled as one.
- 5) A prediction method based on extrapolating the basis vectors of the above BEM representation is finally proposed. Its optimality is established by proving it to be the reduced-rank MMSE estimator of a channel sample outside of the observation interval based on the knowledge of the channel delay-Doppler components within the interval.

### *Outlines*

This paper is organized as follows. Section II provides a general mathematical framework for modeling doubly sparse time-varying wireless channels. Section III is dedicated to a first on-grid approximation of that model and to sparse-recovery channel estimation performance of different waveforms under that approximation. Section IV introduces a relaxation that allows for fractional Doppler frequency shifts along with a new model to capture the associated off-grid effects. Furthermore, the inherent properties of the proposed model are used to enable channel prediction. Finally, numerical results are given in Section V to validate the proposed models and the DS-LTV channel estimation and extrapolation performance of different waveform candidates.

### *Notations*

Bernoulli( $p$ ) is the Bernoulli distribution with probability  $p$  and  $B(n, p)$  is the binomial distribution with parameters  $(n, p)$ . Notation  $X \sim F$  means that random variable  $X$  has distribution  $F$ . If  $\mathcal{A}$  is a set,  $|\mathcal{A}|$  stands for its cardinality. The set of all integers between  $l$  and  $m$  for some  $(l, m) \in \mathbb{Z}^2$  (including  $l$  and  $m$ ) is denoted  $[[l..m]]$ . For a matrix  $\mathbf{M}$ ,  $[\mathbf{M}]_c$  stands for the  $c$ -th column. The ceiling operation is denoted as  $\lceil \cdot \rceil$ . The modulo  $N$  operation is denoted as  $(\cdot)_N$ .

$\mathcal{F}$  stands for the continuous-time Fourier transform operator and  $x \mapsto \text{rect}(x)$  stands for the (standard) rectangular function.  $\mathbf{I}_N$  is the  $N \times N$  identity matrix.

## II. SYSTEM MODEL: LINEAR TIME-VARYING CHANNELS

A linear time-varying (LTV) channel is a model of multipath propagation that is characterized by changes in its impulse response over time, caused by Doppler frequency shifts. The received signal at the channel output corresponding to a signal  $s(t)$  at its input is expressed as:

$$r(t) = \int_{\tau} s(t)h(t, \tau)d\tau + z(t), t \in \mathbb{R}, \quad (1)$$

where  $z(t)$  is the additive white Gaussian noise process and

$$h(t, \tau) = \sum_{p=1}^{N_p} g_p e^{i2\pi\nu_p t \Delta f} \delta(\tau - \tau_p), \quad (2)$$

is the continuous-time impulse response of the channel. Here,  $N_p \geq 1$  is the number of paths,  $\delta(\cdot)$  is the Dirac delta function, and  $g_p, \nu_p$  and  $\tau_p$  are the complex gain, Doppler shift (normalized with respect to the subcarrier spacing  $\Delta f$ ), and the delay (normalized with respect to the sample period  $T_s$ ) associated with the  $p$ -th path, respectively. We define  $\tau_p = l_p + \iota_p$  where  $l_p \in \llbracket 0..L-1 \rrbracket$  is its integer part, while  $\iota_p$  is the fractional part that satisfies  $\frac{-1}{2} < \iota_i \leq \frac{1}{2}$ . We also define  $\nu_p = q_p + \kappa_p$  where  $q_p \in \llbracket -Q..Q \rrbracket$  is its integer part, while  $\kappa_p$  is the fractional part satisfying  $\frac{-1}{2} < \kappa_i \leq \frac{1}{2}$ . In practice, the transmitted signal  $s(t)$  is the continuous-time version of a discrete-time signal  $s_n \triangleq s(nT_s)$  generated from a vector  $\mathbf{x}$  of  $N$  symbols. These symbols could be either data symbols, pilot symbols, or a combination of both. Defining  $r_n \triangleq r(nT_s)$  and  $z_n \triangleq z(nT_s)$ , we get the discrete-time version of the LTV channel model in (1)

$$r_n = \sum_{p=1}^{N_p} g_p e^{i2\pi\nu_p n \Delta f T_s} s(nT_s - \tau_p) + z_n, \quad n \in \mathbb{Z}. \quad (3)$$

From now on, the process  $(z_n)_{n \in \mathbb{Z}}$  is modeled as independent and identically distributed (i.i.d.) with  $z_n \sim \mathcal{CN}(0, \sigma_w^2)$ .

## III. ESTIMATION OF DOUBLY SPARSE LINEAR TIME-VARYING CHANNELS WITH THE ON-GRID APPROXIMATION

### A. First approximation: on-grid doubly sparse linear time-varying channels [16]

In a first approximation, we assume that both  $\iota_p$  and  $\kappa_p$  are zero and we define  $L \triangleq \max_{p=1..N_p} \frac{\tau_p}{T_s} +$

1. Then the discrete-time LTV input-output model in (3) becomes

$$r_n = \sum_{l=0}^{L-1} s_{n-l} h_{l,n} + z_n, \quad n \in \mathbb{Z}. \quad (4)$$

The input-output relation in (4) defines an on-grid LTV channel with a  $L - 1$  maximum delay shift with the complex gain  $h_{l,n}$  of the  $l$ -th path varying with time index  $n$  as

$$h_{l,n} = \sum_{p=1}^{N_p} g_p e^{i2\pi \frac{qn}{N}} \delta_{l-l_p}, l = 0 \dots L - 1. \quad (5)$$

Under this assumption, we assume that  $g_p = \alpha_{l_p, q_p} I_{l_p, q_p}$  where  $I_{l,q}$  is given by:

$$I_{l,q} = \begin{cases} 1 & \text{if } \exists p \text{ such that } (l, q) = (l_p, q_p), \\ 0 & \text{otherwise.} \end{cases} \quad (6)$$

Here,  $I_{l,q}$  for any  $l$  and  $q$  is a binary random variable that, when non-zero, indicates that a channel path with delay  $l$ , Doppler shift  $q$  and complex gain  $\alpha_{l,q}$  is active and contributes to the channel output. The complex gain is assumed to satisfy the channel power normalization

$$\sum_{l=0}^{L-1} \sum_{q=-Q}^Q \mathbb{E} [|\alpha_{l,q}|^2 I_{l,q}] = 1. \quad (7)$$

The number of paths  $N_p$ , in (2) can now be expressed as  $N_p = \sum_{l=0}^{L-1} \sum_{q=-Q}^Q I_{l,q}$ . Note that the distribution of the random variables  $\{I_{l,q}\}_{l,q}$  controls the kind of sparsity the LTV channel might have. We opt for the distribution given by the following definition.

**Definition 1** (On-grid Delay-Doppler double sparsity, [16]). *The complex gain  $h_{l,n}$  of the  $l$ -th path of the LTV channel varies with time as*

$$h_{l,n} = \sum_{q=-Q}^Q \alpha_{l,q} I_{l,q} e^{i2\pi \frac{nq}{N}}, \quad l = 0, \dots, L - 1, \quad (8)$$

and there exist  $0 < p_d, p_D < 1$  such that

$$I_{l,q} = I_l I_q^{(l)}, \quad \forall (l, q) \in \llbracket 0 \dots L - 1 \rrbracket \times \llbracket -Q \dots Q \rrbracket, \quad (9)$$

where  $I_l \sim \text{Bernoulli}(p_d)$  and  $I_q^{(l)} \sim \text{Bernoulli}(p_D)$ . Moreover,  $I_{l,q}$  and  $\alpha_{l,q}$  are independent and  $\alpha_{l,q} \sim \mathcal{CN}(0, \sigma_\alpha^2)$  with  $\sigma_\alpha^2$  satisfying (7).

Note that under Definition 1,  $s_d \triangleq \mathbb{E} [\sum_l I_l] = p_d L$  is the mean number of active delay taps in the delay-Doppler profile of the channel and can be thought of as the *delay domain sparsity level* while  $s_D \triangleq \mathbb{E} [\sum_q I_q^{(l)}] = p_D (2Q + 1)$  is the mean number of active Doppler bins per delay tap and can be thought of as the *Doppler domain sparsity level*. Fig. 1 illustrates three different delay-Doppler sparsity models, fully described in [16] and dubbed Type-1, Type-2 and Type-3, that all fall under the scope of Definition 1 each with an additional different assumption

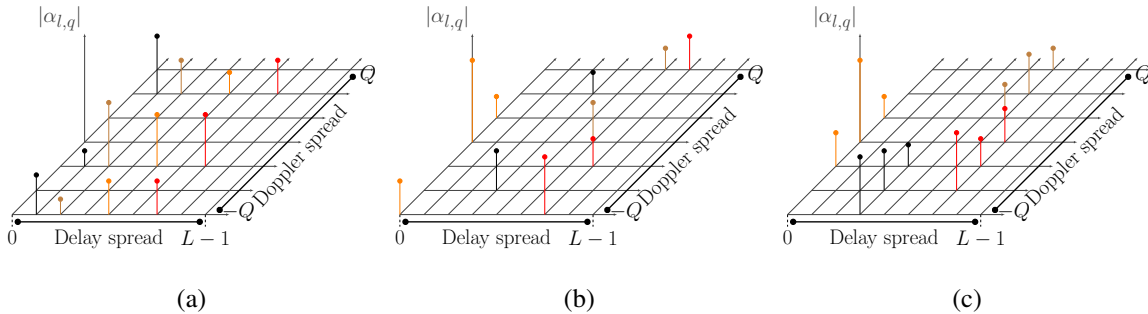


Fig. 1. Examples of channels satisfying (a) Type-1, (b) Type-2, (c) Type-3 delay-Doppler sparsity

on  $I_l$  and  $I_q^{(l)}$ . Here, we just point out that the difference between Type-2 and Type-3 of Figures 1-(b) and 1-(c), respectively, is that in the latter the active Doppler bins per delay tap appear in clusters of random positions but of deterministic length as opposed to the absence of clusters in the former. The case where the delay taps have all the same (random) sparsity (as in Type-1 models of Fig. 1-(a)) also falls under Definition 1 by setting  $I_q^{(l)} = I_q^{(0)}, \forall l$ .

### B. Relation to hierarchical sparsity

**Definition 2** (Hierarchical sparsity, [18]). A vector  $\mathbf{x} \in \mathbb{C}^{NM}$  is  $(s_N, s_M)$ -sparse if it consists of  $N$  blocks of size  $M$ ,  $s_N$  of which at most are non-zero, and each non-zero block is  $s_M$ -sparse.

To analyze hierarchically sparse recovery schemes, a modified version of the restricted isometry property (RIP) called the hierarchical RIP (HiRIP) was proposed in the literature.

**Definition 3** (HiRIP, [18]). The HiRIP constant  $\delta_{s_N, s_M}$  of a matrix  $\mathbf{A}$  is the smallest  $\delta \geq 0$  such that for all  $(s_N, s_M)$ -sparse vectors  $\mathbf{x} \in \mathbb{C}^{NM}$

$$(1 - \delta) \|\mathbf{x}\|^2 \leq \|\mathbf{A}\mathbf{x}\|^2 \leq (1 + \delta) \|\mathbf{x}\|^2 \quad (10)$$

DS-LTV sparsity is probabilistic while hierarchical sparsity of Definition 2 is deterministic. The two models are nonetheless related: if vectorized to a concatenation of its rows, random matrix  $[\alpha_{l,q} I_{l,q}]_{l,q}$  defines a vector  $\alpha \in \mathbb{C}^{(2Q+1)L}$  that consists of  $L$  blocks each of size  $2Q+1$ , where on average  $s_d$  blocks have non-zero entries and where each non-zero block itself is on average  $s_D$ -sparse. To ensure sparsity in a stronger sense i.e., with high probability (as  $L, Q, Lp_d, (2Q+1)p_D$  grow), we require that the following assumption hold.

**Assumption 1.**  $\{I_l\}_{l=0\dots L-1}$  are mutually independent. Moreover, the complementary cumulative distribution function (CCDF)  $\bar{F}_{S_{D,l}}(m)$  of the random variable  $S_{D,l} \triangleq \sum_{q=-Q}^Q I_q^{(l)}$  for any  $l \in \llbracket 0..L-1 \rrbracket$  is upper-bounded for any integer  $m > (2Q+1)p_D$  by the CCDF of  $B(2Q+1, p_D)$ .

Type-1 and 2 models easily satisfy the CCDF upper bound condition simply by requiring that  $\{I_q^{(0)}\}_q$  in the first and  $\{I_q^{(l)}\}_q$  for any  $l$  in the second to be mutually independent (and to thus satisfy  $\bar{F}_{S_{D,l}}(m) = \bar{F}_{B(2Q+1, p_D)}(m), \forall m$ ). For Type-3 models,  $S_{D,l}$  is deterministic and hence its CCDF is trivially upper-bounded. As the following lemma rigorously shows, the mutual independence of  $\{I_l\}_{l=0\dots L-1}$  in Assumption 1 guarantees strong delay domain sparsity while Doppler sparsity is guaranteed in a more explicit manner by the CCDF upper bound.

**Lemma 1.** With probability  $1 - e^{-\Omega(\min((2Q+1)p_D, Lp_d))}$ ,  $\alpha$  is  $(s_d, s_D)$ -sparse under Assumption 1.

*Proof.* The proof (which we first gave in [19]) follows from applying Chernoff's bound to  $S_d$  evaluated at  $s_d = (1 + \epsilon)Lp_d$  and to the  $B(2Q+1, p_D)$  distribution (upper-bounding  $S_D$  as per Assumption 1) evaluated at  $s_D = (1 + \epsilon)(2Q+1)p_D$  with an  $\epsilon > 0$  chosen as small as needed.  $\square$

### C. Compressed-sensing estimation of DS-LTV channels using different waveforms

We now turn our attention to the estimation of the DS-LTV channel using practical waveforms and embedded pilots. For that sake, let  $\mathbf{s}$  be the  $N$ -long vector of samples  $s_n$  at the input of the channel and define  $\mathbf{x}$  as the vector of data symbols and embedded channel estimation pilots that modulate the waveform in use to produce the time-domain samples vector  $\mathbf{s}$ . For all the considered waveforms, we can write the dependence of  $\mathbf{s}$  on  $\mathbf{x}$  using a modulation matrix  $\Phi_{\text{tx}}$

$$\mathbf{s} = \Phi_{\text{tx}} \mathbf{x}. \quad (11)$$

For single-carrier modulation (SCM),  $\Phi_{\text{tx}} = \mathbf{I}_N$ . For AFDM,  $\Phi_{\text{tx}} = \Lambda_{c2} \mathbf{F}_N \Lambda_{c1}$ , with  $\Lambda_c = \text{diag}(e^{-i2\pi cn^2}, n = 0, \dots, N-1)$  and  $\mathbf{F}_N$  being the  $N$ -order discrete Fourier transform (DFT) matrix. For an OFDM grid as the one shown in Figure 3 composed of  $N_s$  symbols each having  $N_{\text{fft}}$  sub-carriers and a cyclic prefix of length  $N_{\text{cp}}$ ,  $\Phi_{\text{tx}} = \text{blkdiag}(\mathbf{T}_{\text{cp}} \mathbf{F}_{N_{\text{fft}}}^H, \dots, \mathbf{T}_{\text{cp}} \mathbf{F}_{N_{\text{fft}}}^H)$  with  $\mathbf{T}_{\text{cp}}$  being the matrix for cyclic prefix insertion. At the receiver, let  $\mathbf{r}$  be the  $N$ -long vector of the channel output samples  $r_n$  defined in (4). Depending on the waveform employed, the receiver applies a demodulation matrix  $\Phi_{\text{rx}}$  to produce the vector of transform domain samples  $\mathbf{y}$ . For both SCM and AFDM,  $\Phi_{\text{rx}} = \Phi_{\text{tx}}^H$ . For the OFDM grid of Figure 3,  $\Phi_{\text{rx}} = \text{blkdiag}(\mathbf{F}_{N_{\text{fft}}} \mathbf{R}_{\text{cp}}, \dots, \mathbf{F}_{N_{\text{fft}}} \mathbf{R}_{\text{cp}})$  and  $\mathbf{R}_{\text{cp}} = [\mathbf{0}, \mathbf{I}_{N_{\text{fft}}}]$  is the matrix for cyclic prefix removal. Let



Tx Frame in time domain:

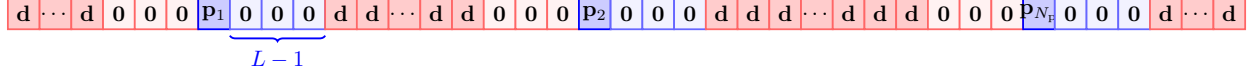


Fig. 2. SCM frame composed of data samples and  $N_p$  pilot symbols, each of the latter surrounded by  $2L - 1$  guard samples.

$\mathcal{P} \subset \llbracket 0..N - 1 \rrbracket$  designate the indexes of the received samples associated with  $N_p$  transform domain pilots, of values  $\{p_p\}_{p=1..N_p}$  inserted at indexes  $\{m_p\}_{p=1..N_p}$  within the vector  $\mathbf{x}$  and each surrounded with a waveform-dependent number of zero guard samples. For SCM (Fig. 2),

$$\mathcal{P} = \bigcup_{p=1}^{N_p} \llbracket m_p..m_p + L - 1 \rrbracket. \quad (\text{SCM}) \quad (12)$$

As for OFDM, let  $m_{p_t} \in \llbracket 0..N_s - 1 \rrbracket$  be the time domain position of the  $p$ -th pilot and  $m_{p_f} \in \llbracket 0..N_{\text{fft}} - 1 \rrbracket$  be its frequency domain position. Then (Fig. 3)

$$\mathcal{P} = \{m_p = m_{t,p_t} N_{\text{fft}} + m_{f,p_f}\}_{\substack{p_t=1..N_{p,t}, \\ p_f=1..N_{p,f}}}, \quad N_p = N_{p,t} N_{p,f}, \quad (\text{OFDM}) \quad (13)$$

While for AFDM, it holds [19] that

$$y_k = \sum_{l=0}^{L-1} \sum_{q=-Q}^Q \alpha_{l,q} I_{l,q} e^{i2\pi(c_1 l^2 - \frac{ml}{N} + c_2(m^2 - k^2))} x_k + w_k, \quad (14)$$

$$m \triangleq (k - q + 2Nc_1 l)_N.$$

The samples related to the  $p$ -th pilot symbol thus occupy  $2N|c_1|(L - 1) + 2Q + 1$  DAFT domain indexes. More precisely, and in case  $c_1$  is negative, then (Fig. 4)

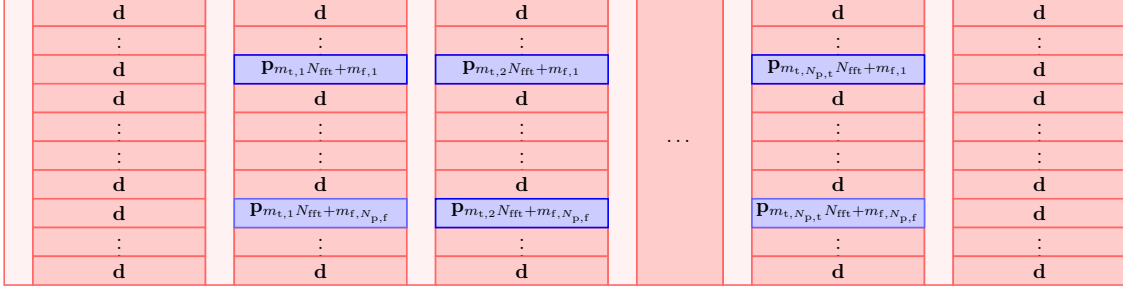
$$\mathcal{P} = \bigcup_{p=1}^{N_p} \llbracket m_p - Q..m_p + 2N|c_1|(L - 1) + Q \rrbracket. \quad (\text{AFDM}) \quad (15)$$

For any of the above waveforms, let  $\mathbf{y}_p \triangleq [y_k]_{k \in \mathcal{P}}$  be the vector of received pilot samples. Inserting (8) and (11) into (4) gives the following signal model for recovery of the hierarchically sparse (per Lemma 1) vector  $\boldsymbol{\alpha}$

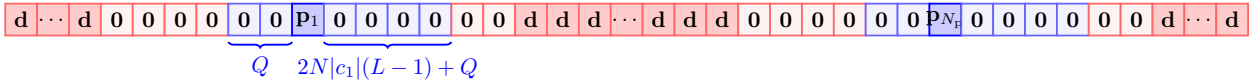
$$\mathbf{y}_p = \underbrace{\mathbf{A}_p \mathbf{M}}_{\triangleq \mathbf{M}_p} \boldsymbol{\alpha} + \mathbf{w}_p \quad (16)$$

where  $[\mathbf{M}]_{l(2Q+1)+Q+q+1} = \boldsymbol{\Phi}_{\text{rx}} \boldsymbol{\Delta}_q \boldsymbol{\Pi}^l \boldsymbol{\Phi}_{\text{tx}}^T \mathbf{x}_p$ ,  $\mathbf{x}_p$  is a vector of the same length as  $\mathbf{x}$  with entries equal to  $p_1, \dots, p_{N_p}$  at indexes  $\{m_p\}_{p=1..N_p}$  and to zero elsewhere, and  $\mathbf{w}_p$  are the corresponding noise samples. Here,  $\mathbf{A}_p$  is the  $|\mathcal{P}| \times N$  matrix that chooses from the transform domain received

Tx Frame in time-frequency domain:

Fig. 3. A frame of  $N_s$   $N_{fft}$ -long OFDM symbols,  $N_{p,t}$  of which having  $N_{p,f}$  pilot subcarriers

Tx Frame in DAFT domain:

Fig. 4. AFDM symbol composed of data samples,  $N_p$  pilot symbols and their guard samples.

vector the entries corresponding to  $\mathcal{P}$ .  $\Delta_q = \text{diag}(e^{i2\pi qn}, n = 0 \dots N - 1)$ ,  $\Pi$  is the  $N$ -order permutation matrix,  $\Phi$  is the transform matrix specific to the waveform.

Hierarchical hard thresholding pursuit (HiHTP) [18] has been suggested in the literature for solving hierarchically-sparse recovery problems. When applied to Problem (16) it gives Algorithm 1. HiHTP employs at each iteration a *hierarchically* sparse thresholding operator

---

**Algorithm 1** HiHTP for compressive sensing of DS-LTV channels
 

---

- 1: **Input:**  $\mathbf{M}_p$ ,  $\mathbf{y}_p$ , maximum number of iterations  $k_{\max}$ ,  $s_d$ ,  $s_D$
  - 2:  $\hat{\alpha}^{(0)} = 0$ ,  $k = 0$
  - 3: **repeat**
  - 4:  $\Omega^{(k+1)} = L_{s_d, s_D}(\alpha^{(k)} + \mathbf{M}_p^H (\mathbf{y}_p - \mathbf{M}_p \alpha^{(k)}))$
  - 5:  $\alpha^{(k+1)} = \arg \min \{ \|\mathbf{y}_p - \mathbf{M}_p \mathbf{z}\|, \text{sup}(\mathbf{z}) \subset \Omega^{(k+1)} \}$
  - 6:  $k = k + 1$
  - 7: **until**  $k = k_{\max}$  or  $\Omega^{(k+1)} = \Omega^{(k)}$  (whichever earlier)
  - 8: **Output:**  $(s_d, s_D)$ -sparse  $\hat{\alpha}^{(k)}$ .
- 

$L_{s_d, s_D}$ . To compute  $L_{s_d, s_D}(\mathbf{x})$  for a vector  $\mathbf{x} \in \mathbb{C}^{L(2Q+1)}$  first a  $s_D$ -sparse approximation is applied to each one of the  $L$  blocks of  $\mathbf{x}$  by keeping in each of them the largest  $s_D$  entries while setting the remaining ones to zero. A  $s_d$ -sparse approximation is next applied to the result by

identifying the  $s_d$  blocks with the largest  $l_2$ -norm. To guarantee the convergence of Algorithm 1 and the recovery of  $\alpha$ , the following technical assumption is needed.

**Assumption 2.**  $\forall l_1 \neq l_2$ , random variables  $\{I_q^{(l_1)}\}_{q=-Q \dots Q}$  are independent of  $\{I_q^{(l_2)}\}_{q=-Q \dots Q}$ .

**Theorem 1** (HiRIP for SCM and OFDM based measurements). *Under Assumption 1 and for sufficiently large  $L, Q$ , sufficiently small  $\delta_t$ , sufficiently small  $\delta_f$ ,  $N_{p,t} = \Omega(\frac{1}{\delta_t^2} \log^2 \frac{1}{\delta_t} \log \frac{s_D}{\delta_t} s_D \log(2Q+1))$  and  $N_{p,f} = \Omega(\frac{1}{\delta_f^2} \log^2 \frac{1}{\delta_f} \log \frac{s_d}{\delta_f} s_d \log L)$ , then the HiRIP constant  $\delta_{s_d, s_D}$  of the SCM measurement matrix  $\mathbf{M}_p$  associated with  $\mathcal{P}(N_{p,t})$  as defined by (12) satisfies  $\delta_{s_d, s_D} \leq \delta_t$  with probability  $1 - e^{-\Omega(\log L \log \frac{s_D}{\delta_t})}$  and the HiRIP constant  $\delta_{s_d, s_D}$  of the OFDM measurement matrix  $\mathbf{M}_p$  associated with  $\mathcal{P} = \mathcal{P}(N_{p,t}, N_{p,f})$  as defined by (13) satisfies  $\delta_{s_d, s_D} \leq \delta_t + \delta_f + \delta_t \delta_f$  with probability  $1 - e^{-\Omega(\min\{\log L \log \frac{s_d}{\delta_t}, \log(2Q+1) \log \frac{s_D}{\delta_f}\})}$ .*

*Proof.* The proof of the theorem is given in Appendix A. □

**Theorem 2** (HiRIP for AFDM based measurements). *Assume  $\Phi_{tx} = \mathbf{\Lambda}_{c2} \mathbf{F}_N \mathbf{\Lambda}_{c1} = \Phi_{rx}^H$ ,  $|c_1| = \frac{P}{2N}$  and let  $P$  be set as the smallest integer satisfying  $(L-1)P + 2Q + 1 \geq s_d s_D$  and  $\mathcal{P} = \mathcal{P}(N_p)$  be defined by (15). Then under Assumptions 1 and 2 and for sufficiently large  $L, Q$ , sufficiently small  $\delta$ , and  $N_p = \Omega(\frac{1}{\delta^2} \log^2 \frac{1}{\delta} \log \frac{\log(LP)}{\delta} \log(LP) \log \frac{Q}{P})$ , the HiRIP constant  $\delta_{s_d, s_D}$  of matrix  $\mathbf{M}_p$  satisfies  $\delta_{s_d, s_D} \leq \delta$  with probability  $1 - e^{-\Omega(\log(2\lceil \frac{Q}{P} \rceil + 1) \log \frac{\log(LP)}{\delta})}$ .*

*Proof.* The proof of the theorem is given in Appendix B. □

When  $P \triangleq 2N|c_1|$  is set to  $2Q + 1$ , AFDM achieves full diversity [15] and the measurements are non-compressive. The setting  $P = 1$ , on the other hand, is the most compressive. By choosing the value of the theorem between these two extremes, each pilot instance gives in its  $(L-1)P + 2Q + 1$ -long guard interval a number of measurements close with high probability to the number  $s_d s_D$  of unknowns. The number  $N_p$  of pilot instances required to estimate the sparsity support has only a logarithmic growth with respect to *both* delay and Doppler spreads. This property is to be contrasted with the SCM and OFDM HiRIP result showing first-degree polynomial dependence of  $N_p$  on  $s_d$  or  $s_D$  as stated by Theorem 1.

**Corollary 1** (Recovery guarantee for compressive sensing of DS-LTV channels). *If  $\mathbf{M}_p$  satisfies the conditions of Theorems 1 or 2, the sequence  $\hat{\alpha}^{(k)}$  defined by Algorithm 1 satisfies  $\|\hat{\alpha}^{(k)} - \alpha\| \leq \rho^k \|\alpha^{(0)} - \alpha\| + \tau \|\mathbf{w}_p\|$  where  $\rho < 1$  and  $\tau$  are constants defined in [18, Theorem 1].*

*Proof.* Thanks to Theorems 1 and 2, matrix  $\mathbf{M}_p$  with large enough  $L, Q, N_p$  can be made to have a HiRIP constant that satisfies  $\delta_{3s_d, 2s_D} < \frac{1}{\sqrt{3}}$ . The conditions of [18, Theorem 1] are thus satisfied, and the corollary follows from that theorem.  $\square$

To get some insights into the above results, we look at them in an asymptotic regime defined with the help of an auxiliary variable  $K$ :  $L \sim K$ ,  $Q \sim K$  ( $L, Q \sim K$  implies  $N \sim K^2$  [16]),  $s_d \sim K^{\kappa_d}$  and  $s_D \sim K^{\kappa_D}$  for some  $\kappa_d, \kappa_D \in [0, 1)$ . In this regime, SCM pilot and guard overhead satisfies  $(2L - 1)N_{p,t} = \Omega((\log K)^2 K^{1+\kappa_D})$  due to Theorem 1. The pilot, guard and CP overhead of OFDM equals  $(L - 1 + N_{p,f})N_{p,t}$ , and is thus smaller than its SCM counterpart but has the same asymptotic growth. As for AFDM, pilot and guard overhead satisfies  $N_p((L - 1)P + 2Q + 1) = \Omega(\log(\log K)(\log K)^2 K)$ . Therefore, under double delay-Doppler sparsity, AFDM overhead is asymptotically dominated by that of OFDM and SCM.

The next section is dedicated to a relaxation of the on-grid approximation to generalize the above results to more realistic propagation and to improve compatibility with channel prediction.

#### IV. ESTIMATION AND EXTRAPOLATION OF DOUBLY SPARSE LINEAR TIME-VARYING CHANNELS WITH OFF-GRID DOPPLER SHIFTS

While the on-grid approximation of Definition 1 is useful for the conception of LTV channel estimation and sensing schemes and for the analysis of their performance as we argued in Section III, it lacks support for the finer Doppler resolution needed for channel prediction or mitigation of channel aging. Indeed, most channel prediction paradigms [20]–[23] involve, explicitly or implicitly, the estimation of Doppler frequency shifts to within an error margin smaller than the frequency resolution characteristic of the duration of the channel observation interval. For that sake, we now present a second approximation for LTV channels that allows, in contrast to the first approximation in Definition 1, for fractional-valued Doppler frequency shifts.

##### *A. Off-grid doubly sparse linear time-varying channels*

We now allow for fractional-valued Doppler frequency shifts. In this case, only  $\iota_p$  is zero, while  $\kappa_p$  may take non-zero values sampled from a uniform distribution i.e.,  $\kappa_p \sim \mathcal{U}([-\frac{1}{2}, \frac{1}{2}])$ . Define  $N_{D,l,q}$  as the number of “sub”-paths with the same delays and Doppler shifts integer part and which only differ in their Doppler shifts fractional part:

$$N_{D,l,q} \triangleq |\{p \in \llbracket 1 \dots N_p \rrbracket \mid l_p = l, q_p = q\}|. \quad (17)$$

In this configuration, the number of paths  $N_p$  in (2) satisfies  $N_p = \sum_{l=0}^{L-1} \sum_{q=-Q}^Q N_{D,l,q} I_{l,q}$ . Depending on the scenario, it is in principle possible to model  $N_{D,l,q}$  either as a fixed value or as a random variable, for example, a uniform random variable drawn over the range  $\llbracket 1..N_D \rrbracket$ . For simplicity, we opt for the first option, that is,  $N_{D,l,q} = N_D, \forall l, q$  for some value  $N_D$  and we impose that the following channel power normalization should be satisfied.

$$\sum_{l=0}^{L-1} \sum_{q=-Q}^Q \sum_{i=1}^{N_D} \mathbb{E} [|\alpha_{l,q,i}|^2 I_{l,q}] = 1. \quad (18)$$

**Definition 4** (off-grid Delay-Doppler double sparsity). *The complex gain  $h_{l,n}$  of the  $l$ -th path of the LTV channel varies with time as*

$$h_{l,n} = \sum_{q=-Q}^Q I_{l,q} \sum_{i=1}^{N_D} \alpha_{l,q,i} e^{i2\pi \frac{n(q+\kappa_i)}{N}}, \quad l = 0 \dots L-1 \quad (19)$$

for some value  $N_D$ , with  $I_{l,q}$  retaining the same description provided in Definition 1 and with  $I_{l,q}, \{\alpha_{l,q,i}, \kappa_i\}_{i=1..N_D}$  being mutually independent. The complex gains are assumed to satisfy  $\alpha_{l,q,i} \sim \mathcal{CN}(0, \sigma_\alpha^2)$  with  $\sigma_\alpha^2$  chosen so that (18) is respected.

Figure 5 illustrates possible realizations of the above model. Note that the given examples can be seen as an off-grid relaxation of the three sparsity profiles from Figure 1.

**Remark 1.** *Maintaining the delay taps as integer values is not to the detriment of the core message of this work since the same approach we develop to deal with off-grid Doppler shifts can be extended to off-grid delays. Moreover, the effect of off-grid delays can still be made to fall under the current model by increasing the value of the model delay domain sparsity parameter  $p_d$  sufficiently to account for leakage due to the fractional part of the delay shifts.*

Estimating all the unknown parameters of the off-grid channel model in (19) remains a challenging task. Indeed, the  $N_D$  Doppler frequency shifts  $\{q + \kappa_i\}_{i=1..N_D}$  associated with a grid point  $(l, q)$  are only different by their fractional part and hence render the problem of estimating the corresponding complex coefficients  $\{\alpha_{l,q,i}\}_{i=1..N_D}$  ill-conditioned. Moreover, the number of unknowns in the model i.e.,  $N_p$ , could be prohibitively large. For both these reasons, we propose a new model based on multiple “elementary” basis expansion models (BEM), each set with a bandwidth equal to the frequency resolution and shifted in frequency to be centered at one of the active grid points. Thanks to its optimality in terms of time-frequency localization [24], we opt for BEM based on discrete prolate spheroidal sequences (DPSS).

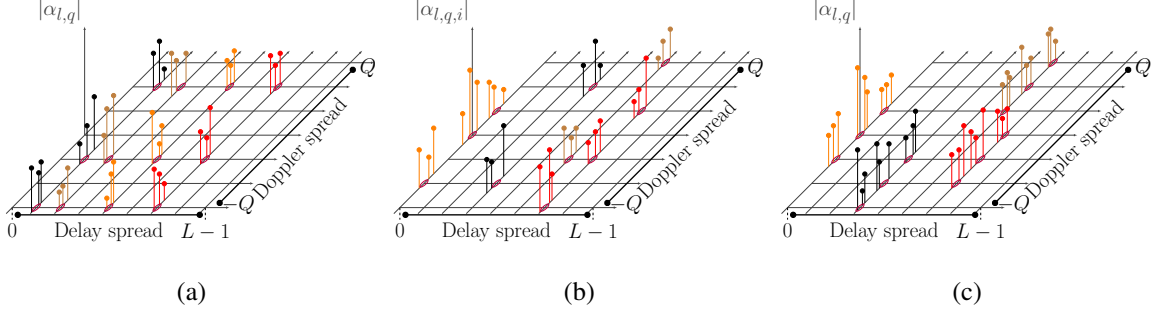


Fig. 5. Three Instances of the delay-Doppler domain response of a DS-LTV channel satisfying Definition 4 and (a) off-grid Type-1, (b) off-grid Type-2, (c) off-grid Type-3 delay-Doppler sparsity

### B. Background: DPSS Basis Expansion Model

We begin with an overview of DPSS BEM modeling of a baseband signal  $h_n$  that occupies a bandwidth  $(-W, W)$  in digital frequencies with  $W \in (0, \frac{1}{2})$ . DPSS basis vectors  $u_{b,n}^{(N,W)}$  ( $b = 1, \dots, N$ ) are the eigenvectors of the prolate matrix [25]:

$$\sum_{k=0}^{N-1} C_{k,n}^{(N,W)} u_{b,k}^{(N,W)} = \lambda_b^{(N,W)} u_{b,n}^{(N,W)}, b = 1 \dots N, n = 0 \dots N - 1 \quad (20)$$

where  $C_{k,n}^{(N,W)}$  is the  $(k - n)$ -th entry of the prolate matrix:

$$C_{k,n}^{(N,W)} = \frac{\sin(2\pi W(k - n))}{\pi(k - n)}. \quad (21)$$

The eigenvectors are normalized so that  $\sum_{n=1}^N \left(u_{b,n}^{(N,W)}\right)^2 = 1$ . The eigenvalues are ordered according to their values starting with the largest one:  $1 \geq \lambda_0^{(N,W)} \geq \dots \geq \lambda_{N-1}^{(N,W)} \geq 0$ . The eigenvalues  $\lambda_b^{(N,W)}$  (representing energy concentration) are clustered near 1 for  $b \leq 2WN$ , and rapidly drop to zero for  $b > 2WN$  [26]. In this study we employ multiple DPSS BEMs, each of which is used to represent the channel signal component related to the fractional part of the  $N_D$  Doppler shifts around one of the grid points  $(l, q)$  i.e.,  $\sum_{i=1}^{N_D} \alpha_{l,q,i} e^{j2\pi \frac{n\kappa_i}{N}}$ , and not the channel signal associated with the whole Doppler spread i.e.,  $h_{l,n}$ . Each of these BEMs is defined using (20) and (21) with  $W = \frac{1}{2N}$ . In the interest of simplicity, all parameters with the superscript  $(N, W)$  in their notation, such as  $u_{b,n}^{(N,W)}$ , will be replaced by their simplified forms e.g.,  $u_{b,n}$ .

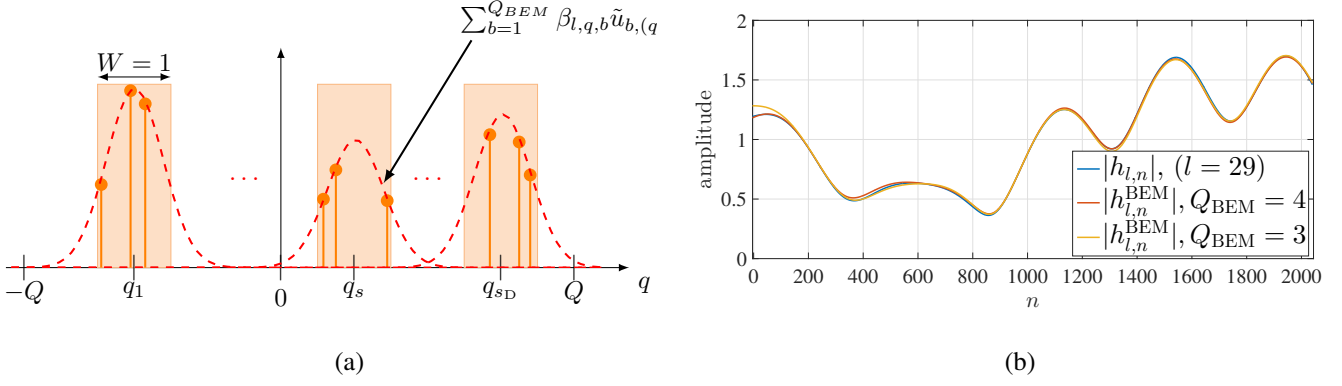


Fig. 6. (a) Capturing the leakage due to  $S_D$  clusters of off-grid Doppler shifts  $\{q_s + \kappa_i\}_{s=1 \dots S_D, i=1 \dots N_D}$ , by  $S_D$  frequency shifted copies of a DPSS BEM  $\{u_{b,n}\}_{b=1 \dots Q_{\text{BEM}}}$  ( $\tilde{u}_{b,k}$  in the figure being the DFT of  $u_{b,n}$ ). (b) Absolute-value comparison between a DS-LTV channel  $h_{l,n}$  having  $S_D = 3$  Doppler shift clusters and its representation using 3 elementary shifted BEMs with  $Q_{\text{BEM}} = 3$  and  $Q_{\text{BEM}} = 4$  ( $N = 2048$ ,  $W = \frac{1}{2N}$ ,  $Q = 7$ )

### C. Off-grid approximation using multiple shifted elementary BEMs

The following term in (19) represents a signal occupying a frequency band centered at digital frequency  $\frac{q}{N}$  and of a bandwidth equal to  $\frac{1}{N}$

$$h_{l,q,n} \triangleq \sum_{i=1}^{N_D} \alpha_{l,q,i} e^{i2\pi \frac{n(q+\kappa_i)}{N}} \quad (22)$$

Its baseband version defined as  $e^{-i2\pi \frac{nq}{N}} h_{l,q,n}$  can thus be modeled (see Figure 6) using a DPSS BEM of an order equal to  $Q_{\text{BEM}}$  (chosen large enough depending on the required modeling precision) and a bandwidth  $(-W, W)$  with  $W = \frac{1}{2N}$  by defining

$$h_{l,q,n}^{\text{BEM}} \triangleq e^{i2\pi \frac{nq}{N}} \sum_{b=1}^{Q_{\text{BEM}}} \beta_{l,q,b} u_{b,n}. \quad (23)$$

In vector form

$$\boldsymbol{\beta}_{l,q} = \mathbf{U}_{Q_{\text{BEM}}}^H \mathbf{E}_{\frac{q}{N}}^H \mathbf{h}_{l,q} \quad (24)$$

$$\mathbf{h}_{l,q}^{\text{BEM}} = \mathbf{E}_{\frac{q}{N}} \mathbf{P}^{\text{BEM}} \mathbf{E}_{\frac{q}{N}}^H \mathbf{h}_{l,q} \quad (25)$$

with  $\mathbf{U}_{Q_{\text{BEM}}} \triangleq [\mathbf{u}_1 \dots \mathbf{u}_{Q_{\text{BEM}}}]$  and  $\mathbf{P}^{\text{BEM}} = \mathbf{U}_{Q_{\text{BEM}}} \mathbf{U}_{Q_{\text{BEM}}}^H$  being the orthogonal projection matrix associated with the DPSS BEM representation and  $\mathbf{E}_f \triangleq \text{diag}(e^{i2\pi f_0} \dots e^{i2\pi f(N-1)})$ .

Inserting the elementary BEMs defined in (23) for each Doppler grid point into (19) gives

$$\begin{aligned} h_{l,n}^{\text{BEM}} &= \sum_{q=-Q}^Q I_{l,q} e^{i2\pi \frac{nq}{N}} \sum_{b=1}^{Q_{\text{BEM}}} \beta_{l,q,b} u_{b,n}, \\ &= \sum_{q=-Q}^Q I_{l,q} h_{l,q,n}^{\text{BEM}}, \quad l = 0 \dots L-1 \quad (\text{“multiple shifted elementary BEMs” model}) \end{aligned} \quad (26)$$

The precision of the above representation in relation to the order of the elementary BEMs in the model (26) is provided by the following theorem.

**Theorem 3.** *For any  $\epsilon > 0$ , if we set  $Q_{\text{BEM}} \geq C \log \frac{1}{\epsilon}$  for some constant  $C$  then the representation error of the model in (26) satisfies  $\sum_{l=0}^{L-1} \mathbb{E} \left[ |h_{l,n} - h_{l,n}^{\text{BEM}}|^2 \right] < \epsilon$  for a sufficiently large  $N$ .*

*Proof.* The proof of Theorem 3 is given in Appendix C. □

Theorem 3 states that the number of DPSS basis functions needed to represent the channel component associated with a single delay-Doppler grid point grows only logarithmically with the inverse of the target precision. The following figure (as well as the numerical results of Section V) shows that as few as 4 DPSS basis functions ( $Q_{\text{BEM}} = 4$ ) are sufficient to get good enough precision. Note that this value is unrelated to the Doppler spread value i.e.,  $2Q + 1$ : a larger Doppler spread does not imply the need for a larger value of  $Q_{\text{BEM}}$ .

#### D. DS-LTV off-grid channel estimation

Let  $\beta$  be the vectorized form of the BEM coefficients  $\{\beta_{l,q,b}\}_{\substack{b=1 \dots Q_{\text{BEM}} \\ l,q,I_{l,q} \neq 0}}$  associated with the active delay-Doppler grid points. Note that the knowledge of the delay-Doppler sparsity support i.e., of  $\{I_{l,q}\}_{l=0 \dots L-1, q=-Q \dots Q}$ , at the receiver side is now assumed. Define  $\mathbf{B}$  as the following block-diagonal matrix

$$\mathbf{B} = \text{blkdiag} \left( \tilde{\mathbf{B}}_0, \dots, \tilde{\mathbf{B}}_{L-1} \right) \quad (27)$$

with  $\tilde{\mathbf{B}} \triangleq [\tilde{\mathbf{B}}_{-Q} \dots \tilde{\mathbf{B}}_Q]$  being a  $N \times (2Q + 1)Q_{\text{BEM}}$  matrix satisfying  $[\tilde{\mathbf{B}}_q]_{n,b} = \frac{1}{\sqrt{N}} \tilde{U}_{b,(n-q)}$  and  $\tilde{U}_{b,n} = \frac{1}{\sqrt{N}} \sum_{k=0}^{N-1} u_{b,k} e^{-i2\pi \frac{nk}{N}}$  being the DFT of the DPSS basis vector  $u_{b,n}$ . Let  $\mathbf{A}_\beta$  be the matrix that places the blocks of  $\beta$ , each of size  $Q_{\text{BEM}}$ , within the positions corresponding to  $I_{l,q} \neq 0$  in a larger vector of length  $LQ_{\text{BEM}}(2Q + 1)$  resulting in a  $LQ_{\text{BEM}}(2Q + 1)$ -long vector  $\mathbf{A}_\beta \beta$  that is block sparse. Now, define

$$\alpha \triangleq \mathbf{B} \mathbf{A}_\beta \beta. \quad (28)$$



Inserting (28) into (16), we can write the received pilot samples vector  $\mathbf{y}_p$  as

$$\mathbf{y}_p = \underbrace{\mathbf{A}_p \mathbf{M} \mathbf{B} \mathbf{A}_\beta}_{\triangleq \mathbf{M}_p} \boldsymbol{\beta} + \mathbf{w}_p. \quad (29)$$

where  $\mathbf{M}$  and  $\mathbf{A}_p$  are defined in (16). The minimum mean squared error (MMSE) estimate,  $\hat{\boldsymbol{\beta}}$ , of  $\boldsymbol{\beta}$  based on  $\mathbf{y}_p$  is given by [27] as

$$\hat{\boldsymbol{\beta}} = \mathbf{B} (\sigma_\alpha^2 \mathbf{M}_p^H \mathbf{M}_p + \sigma_w^2 \mathbf{I})^{-1} \mathbf{M}_p^H \mathbf{y}_p. \quad (30)$$

Finally, define

$$\hat{h}_{l,n}^{\text{BEM}} = \sum_{q=-Q}^Q I_{l,q} e^{j2\pi \frac{nq}{N}} \sum_{b=1}^{Q_{\text{BEM}}} \hat{\beta}_{l,q,b} u_{b,n}, \quad n = 0, \dots, N-1. \quad (31)$$

as the resulting MMSE estimate of  $h_{l,n}^{\text{BEM}}$ . In vector form

$$\hat{\mathbf{h}}_l^{\text{BEM}} = \sum_{q=-Q}^Q I_{l,q} \underbrace{\mathbf{E}_{\frac{q}{N}} \mathbf{U}_{Q_{\text{BEM}}}}_{\triangleq \hat{\mathbf{h}}_{l,q}^{\text{BEM}}} \hat{\boldsymbol{\beta}}. \quad (32)$$

The mean squared error (MSE) conditioned on a given  $I_{l,q}$  realization is then written as

$$\begin{aligned} \sum_{l=0}^{L-1} \frac{1}{N} \mathbb{E} \left[ \left\| \mathbf{h}_l^{\text{BEM}} - \hat{\mathbf{h}}_l^{\text{BEM}} \right\|^2 \right] &\leq \frac{1}{N} \sum_{l=0}^{L-1} \sum_{q=-Q}^Q I_{l,q} \mathbb{E} \left[ \left\| \mathbf{h}_{l,q}^{\text{BEM}} - \hat{\mathbf{h}}_{l,q}^{\text{BEM}} \right\|^2 \right] \\ &= \frac{1}{N N_D \sigma_\alpha^2} \mathbb{E} \left[ \left\| \boldsymbol{\beta} - \hat{\boldsymbol{\beta}} \right\|^2 \right] \end{aligned} \quad (33)$$

where the inequality is due to the triangle inequality and where the equality is due to the definition of  $\hat{\mathbf{h}}_{l,q}^{\text{BEM}}$  in (32), to the fact that  $\sum_{l=0}^{L-1} \sum_{q=-Q}^Q I_{l,q} = \frac{1}{N_D \sigma_\alpha^2}$  per (18) and to the fact that  $\mathbf{E}_{\frac{q}{N}}^H \mathbf{E}_{\frac{q}{N}} = \mathbf{I}_N$  and  $\mathbf{U}_{Q_{\text{BEM}}}^H \mathbf{U}_{Q_{\text{BEM}}} = \mathbf{I}_{Q_{\text{BEM}}}$ .

**Assumption 3.** *The number  $N_p$  of pilots is sufficiently large for the MSE associated with estimating  $\boldsymbol{\beta}$  (and hence  $\mathbf{h}_l^{\text{BEM}}$  per (33)) to converge to zero as  $\sigma_w^2 \rightarrow 0$ .*

**Remark 2** (Impact of the sensing waveform). *The value of  $N_p$  needed for Assumption 3 to hold depends on the particular waveform in use. The numerical results given in Section V show that the relative advantage of AFDM over OFDM and SCM, which has been analytically established by Theorems 1 and 2 under the on-grid channel model, is still valid in the off-grid case.*

Assumption 3 is about the MSE of estimating the BEM representation of the channel. The following corollary to Theorem 3 provides an analysis of the estimation MSE when computed with respect to the actual channel defined by (4) instead of its BEM representation.

**Corollary 2.** *Under Assumption 3 and Definition 4, provided that  $N$  is large enough and  $Q_{\text{BEM}} \geq C \log \frac{1}{\epsilon}$  for any  $\epsilon > 0$  and some constant  $C$ , then  $\lim_{\sigma_w^2 \rightarrow 0} \mathbb{E} \left[ \sum_{l=0}^{L-1} \frac{1}{N} \left\| \mathbf{h}_l - \hat{\mathbf{h}}_l^{\text{BEM}} \right\|^2 \right] \leq \epsilon$ .*

*Proof.* Apply the triangle inequality to  $\mathbf{h}_l - \hat{\mathbf{h}}_l^{\text{BEM}} = (\mathbf{h}_l - \mathbf{h}_l^{\text{BEM}}) + (\mathbf{h}_l^{\text{BEM}} - \hat{\mathbf{h}}_l^{\text{BEM}})$  followed by applying Assumption 3 to the first term and Theorem 3 to the second.  $\square$

### E. Application to channel extrapolation and prediction

We know from the literature on the Slepian basis [23] that there is a “natural” way to extend the finite sequences  $u_{b,n}$  from the smaller interval  $\llbracket 0..N-1 \rrbracket$  to the larger one  $\llbracket -N_{\text{ext}}..N+N_{\text{ext}} \rrbracket$ , where  $N_{\text{ext}}$  denotes the additional channel samples to be extrapolated. This is achieved by letting the index  $n$  in (20) be defined over  $\mathbb{Z}$  instead of being confined to  $\llbracket 0..N-1 \rrbracket$  leading to

$$u_{b,n}^{\text{ext}} \triangleq \frac{1}{\lambda_b^{(N,W)}} \sum_{k=0}^{N-1} C_{k,n}^{(N,W)} u_{b,k}, n \in \mathbb{Z}. \quad (34)$$

Signal  $(u_{b,n}^{\text{ext}})_{n \in \mathbb{Z}}$  (“ext” stands for “extrapolation”) has a discrete-time Fourier transform (DTFT) that is zero outside  $(-W, W)$  and is the signal that has the least energy outside the time interval  $\llbracket 0..N-1 \rrbracket$  from among all the discrete-time signals band-limited to  $(-W, W)$  [23].

Once we have estimated the multiple-BEM representation of the off-grid DS-LTV channel on the interval  $\llbracket 0..N-1 \rrbracket$  as in (31) and once we have calculated the infinite-time version of the DPSS basis function as in (34), the channel can thus be extrapolated as follows

$$h_{l,n}^{\text{ext}} \triangleq \sum_{q=-Q}^Q I_{l,q} e^{i2\pi \frac{nq}{N}} \underbrace{\sum_{b=1}^{Q_{\text{BEM}}} \hat{\beta}_{l,q,b} u_{b,n}^{\text{ext}}}_{\triangleq h_{l,q,n}^{\text{ext}}}, l = 0 \dots L-1, n \in \mathbb{Z}. \quad (35)$$

Here, we defined

$$h_{l,q,n}^{\text{ext}} \triangleq e^{i2\pi \frac{nq}{N}} \sum_{b=1}^{Q_{\text{BEM}}} \hat{\beta}_{l,q,b} u_{b,n}^{\text{ext}}. \quad (36)$$

Defining  $\mathbf{u}_n^{\text{ext}} \triangleq [u_{1,n}^{\text{ext}} \dots u_{Q_{\text{BEM}},n}^{\text{ext}}]^T$  and referring to (32) gives

$$h_{l,q,n}^{\text{ext}} = e^{i2\pi \frac{nq}{N}} (\mathbf{u}_n^{\text{ext}})^T \mathbf{U}_{Q_{\text{BEM}}}^H \mathbf{E}_{\frac{q}{N}}^H \hat{\mathbf{h}}_{l,q}^{\text{BEM}} \quad (37)$$

it is known [24] that the  $b$ -th infinite-length DPSS has  $1 - \lambda_b^{(N,W)}$  (respectively  $\lambda_b^{(N,W)}$ ) of its energy outside (respectively inside) the interval  $\llbracket 0..N-1 \rrbracket$  as illustrated in Figure 7. Therefore, the terms of the sum that contribute the most to the value of  $h_{l,q,n}^{\text{ext}} = e^{i2\pi \frac{nq}{N}} \sum_{b=1}^{Q_{\text{BEM}}} \beta_{l,q,b} u_{b,n}^{\text{ext}}$  for  $n > N-1$  are the ones with large enough samples  $u_{b,n}^{\text{ext}}$  i.e., with small enough  $\lambda_b^{(N,W)}$ .

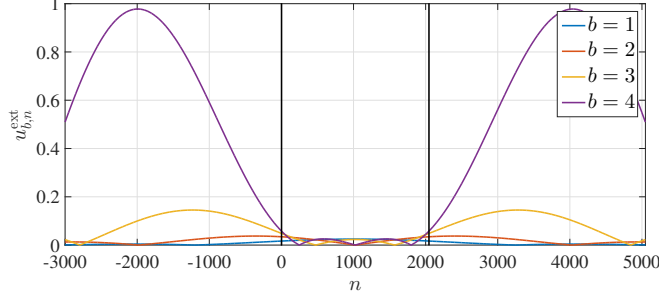


Fig. 7. Extrapolated versions of the first four DPSS ( $N = 2048$ ,  $W = \frac{1}{2N}$ )

While this constrains  $Q_{\text{BEM}}$  to be sufficiently large, it simultaneously constrains the estimation SNR to be high enough to guarantee a precise estimation of coefficients  $\beta_{l,q,b}$  associated with basis functions that have little contribution to the signal received inside the observation interval  $\llbracket 0..N-1 \rrbracket$ . The issue of setting the value of  $Q_{\text{BEM}}$  is further discussed in Section V.

The following theorem establishes the optimality in a certain sense of the predictor  $h_{l,n}^{\text{ext}}$  by relating it to a reduced-rank MMSE estimator.

**Theorem 4.** *The predictor  $h_{l,n}^{\text{ext}}$  defined by (35) for any  $n > N - 1$  based on extrapolating multiple estimated BEMs of order  $Q_{\text{BEM}}$  converges in the squared-mean sense in the limit of a vanishing noise variance to a reduced-rank (with a reduced rank equal to  $Q_{\text{BEM}}$ ) MMSE estimator of sample  $h_{l,n}$  under the assumptions of Definition 4 and Assumption 3.*

*Proof.* The proof of Theorem 4 is given in Appendix D. □

**Remark 3** (Relation to other DPSS extrapolation prediction methods). *The DPSS-based BEM modeling in [23] uses a single BEM of order  $\tilde{Q}_{\text{BEM}}$  to represent the multi-band signal  $h_{l,n} = \sum_{q=-Q}^Q I_{l,q} \sum_{i=1}^{N_{\text{D}}} \alpha_{l,q,i} e^{i2\pi \frac{n(q+\kappa_i)}{N}}$  of each channel delay tap to give*

$$\check{h}_{l,n}^{\text{BEM}} = \sum_{b=1}^{\tilde{Q}_{\text{BEM}}} \check{\beta}_{l,q,b} \check{u}_{b,n}, \quad n = 0, \dots, N-1. \quad (38)$$

where  $\check{u}_{b,k}^{(N,W)}$  are the basis vectors of the single multi-band BEM defined as

$$\sum_{k=0}^{N-1} \check{C}_{k,n}^{(N,W)} \check{u}_{b,k} = \check{\lambda}_b^{(N,W)} \check{u}_{b,n}, \quad b = 1 \dots N, n = 0 \dots N-1, \quad (39)$$

$$\check{C}_{k,n}^{(N,W)} \triangleq \sum_{\substack{q=-Q \\ I_{l,q}=1}}^Q e^{i2\pi \frac{q(k-n)}{N}} \frac{\sin(2\pi W(k-n))}{\pi(k-n)}. \quad (40)$$

The associated channel predictor is

$$\check{h}_{l,n}^{\text{ext}} \triangleq \sum_{b=1}^{\check{Q}_{\text{BEM}}} \check{\beta}_{l,q,b} \check{u}_{b,n}^{\text{ext}}, \quad l = 0 \cdots L-1, \quad n \in \mathbb{Z}, \quad (41)$$

where the associated extrapolated basis vector is given by

$$\check{u}_{b,n}^{\text{ext}} \triangleq \frac{1}{\check{\lambda}_b^{(N,W)}} \sum_{k=0}^{N-1} \check{C}_{k,n}^{(N,W)} \check{u}_{b,k}, \quad n \in \mathbb{Z}. \quad (42)$$

The main issue with the multi-band DPSS approach is the size of the codebook that needs to be computed or stored at the network device performing the channel estimation. As can be seen from (29), the codebook size in our approach is the number of columns of the matrix  $\mathbf{MB}$  which equals  $Q_{\text{BEM}}L(2Q+1)$ . In the case of the multi-band BEM approach, the codebook size would be  $L \sum_{k=1}^{2Q+1} \binom{2Q+1}{k} \check{Q}_{\text{BEM}}(k) \gg Q_{\text{BEM}}L(2Q+1)$  as every different combination of  $k$  active Doppler grid points would result in a different multi-band prolate matrix  $\check{C}_{k,n}^{(N,W)}$  (40) and thus in a different DPSS basis (39). Another advantage of the multiple shifted BEMs scheme is the fact that we can analytically quantify its precision, as we did in Theorem 3 and Corollary 2.

## V. NUMERICAL RESULTS

We first present the results pertaining to the estimation of DS-LTV channels with the on-grid approximation of Definition 1. AFDM sparse recovery performance is compared to that of OFDM and OTFS. We used 100 realizations of channels having a Type-1 delay-Doppler sparsity with  $p_d = 0.2$ ,  $p_D \in \{0.2, 0.4\}$  and  $N = 4096$ ,  $L = 30$ ,  $Q = 7$  (corresponding to a 30 MHz transmission at a 70 GHz carrier frequency, a maximum target moving speed of 396 km/h and a maximum target range of 300 meters). For both OFDM and AFDM, sparse recovery of  $\alpha$  is done using HiHTP (Algorithm 1) based on the pilot pattern described in Figures 3 and 4, respectively. For OTFS, since sensing is done without compression, non-compressive estimation algorithms can be used [15]. For each waveform, the pilot overhead was set in such a way that the mean squared error  $\text{MSE} \triangleq \mathbb{E}[\|\hat{\alpha} - \alpha\|^2]$  is approximately  $10^{-4}$  at  $\text{SNR} = 20$  dB. Fig. 8 shows an advantage of AFDM in terms of pilot overhead i.e., the number of samples in each frame needed as pilots and guards to achieve the target MSE performance. This performance validates the theoretical result given in Theorems 1 and 2 implying that the overhead needed to get the same HiRIP level is smaller for AFDM compared to SCM and OFDM.

We now turn to the estimation and extrapolation of DS-LTV channels with off-grid Doppler shifts as modeled by Definition 4. We start with the configuration of our BEM model proposed

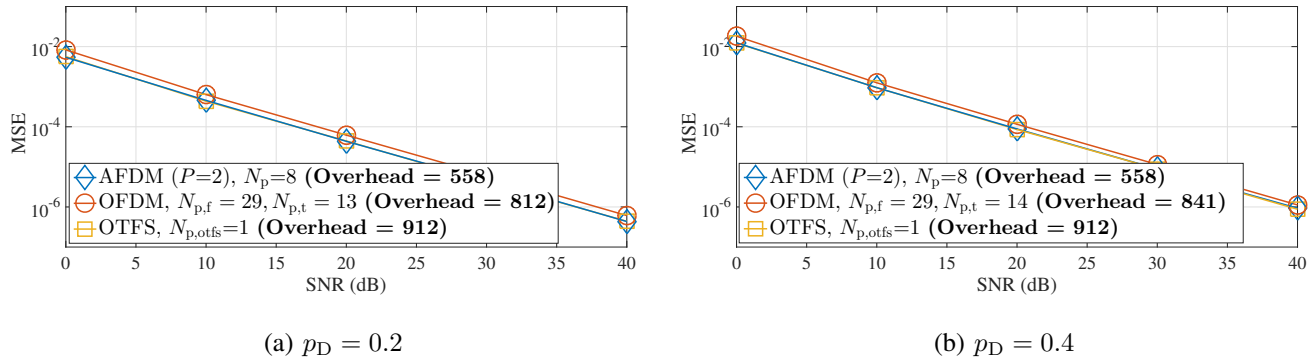


Fig. 8. MSE and pilot overhead for  $N = 4096, L = 30, Q = 7, p_d = 0.2, N_{\text{ofdm, symb}} = 16, N_{\text{otfs}} = 16, M_{\text{otfs}} = 256$ . Overhead:  $N_{\text{p, td}}N_{\text{p, fd}} + (N_{\text{ofdm, symb}} - 1)(L - 1)$  for OFDM,  $\min(4Q + 1, N_{\text{otfs}})\min(2L - 1, M_{\text{otfs}})$  for OTFS,  $N_p((L - 1)P + 1) + (L - 1)P + 4Q$  for AFDM.

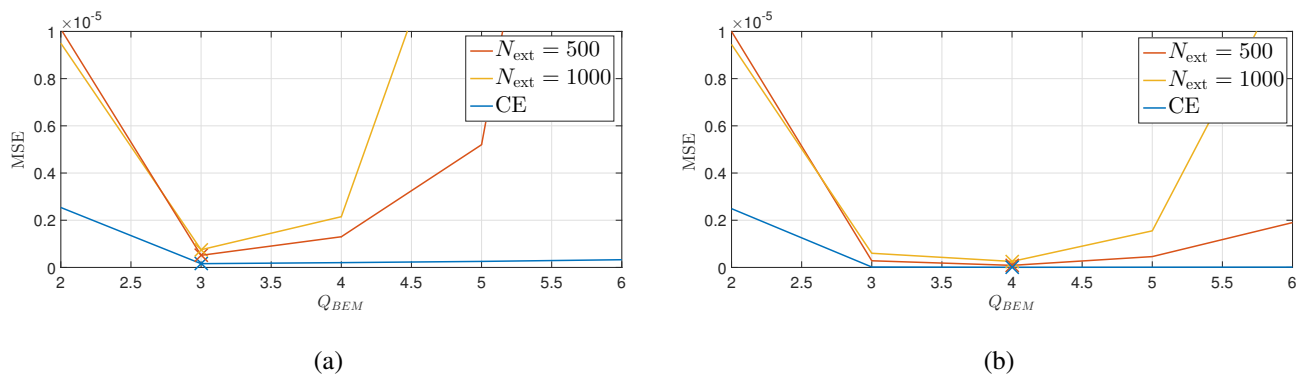


Fig. 9. MSE as function of  $Q_{\text{BEM}}$  for the estimation of a channel tap with one cluster of fractional Doppler shifts ( $N = 2048, Q = 7, N_p = 46$ ) for two SNR values (a) SNR = 10 dB, (b) SNR = 40 dB

in Subsection IV-C. The effect of the order  $Q_{\text{BEM}}$  of the elementary BEM on the MSE with different extrapolation horizons, namely  $N_{\text{ext}} = 1000, N_{\text{ext}} = 500$  and  $N_{\text{ext}} = 0$  (marked as CE), is shown in Figure 9. While increasing  $Q_{\text{BEM}}$  improves the precision of the model, it increases the number of unknown to be estimated revealing the trade-off between model precision and estimation performance. This is why  $Q_{\text{BEM}} = 3$  yields the best MSE at the lower SNR value as opposed to  $Q_{\text{BEM}} = 4$  at the higher. Note that both of these two  $Q_{\text{BEM}}$  values being small confirm the result given in Theorem 3.

Figure 10 compares the MSE performance of our method based on multiple shifted elementary BEMs with  $Q_{\text{BEM}} = 4$  to two other approaches, namely the single-BEM approach of (39) (configured such that  $\frac{Q_{\text{BEM}}}{\# \text{ active Doppler shifts per delay tap}} = 4$ ), and a refined-grid approach [6] (with a refinement factor of  $O = 4$ ). The comparison is done for both channel estimation and prediction

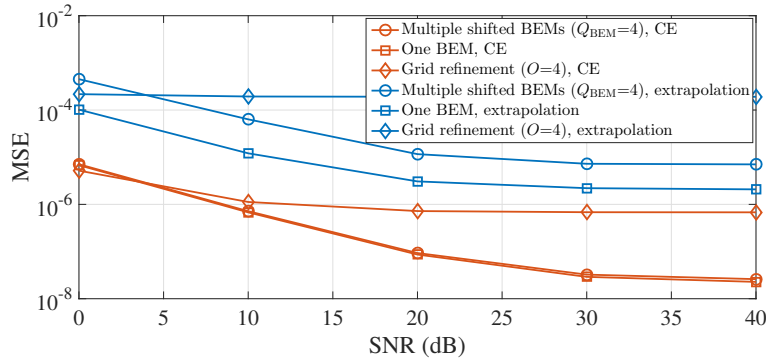


Fig. 10. MSE performance of AFDM using different approaches ( $N = 2048, L = 20, Q = 7, p_d = 0.2, p_D = 0.2$ )

TABLE I  
SIZE OF CODEBOOK FOR EACH METHOD

Method	Codebook Size
One BEM	2,621,360
Multiple BEMs	1,200

assuming  $N_{\text{ext}} = 500$  and the underlying waveform is AFDM with  $P = 1$ . The values of  $Q_{\text{BEM}}$ ,  $\tilde{Q}_{\text{BEM}}$ , and  $O$  are chosen equal to ensure a fair comparison across all methods, both in terms of model size (number of unknown parameters) and computational complexity. For channel estimation, the multiple shifted BEMs approach and the single-BEM method achieve similar performance, both outperforming the refined-grid technique (due to the latter being ill-conditioned since  $N_D > 1$  as explained at the beginning of Section IV). However, for channel prediction, our approach exhibits a slight performance degradation compared to the single BEM method. Nevertheless, as highlighted in Remark 3, our method requires a significantly smaller codebook size than the single BEM approach shown by Table I (for the same setting as in Figures 11 and 10), making it more efficient in practical implementations.

Finally, we shift our attention to comparing the sparse recovery performance of AFDM with that of OFDM. We used 100 realizations of channels having a off-grid Type-1 delay-Doppler sparsity with  $p_d = 0.2, p_D = 0.2$  and  $N = 2048, L = 20, Q = 7$  (corresponding to a 15 MHz transmission at a 70 GHz carrier frequency, a maximum target moving speed of 396 km/h and a maximum target range of 400 meters). As highlighted previously in remark 2,

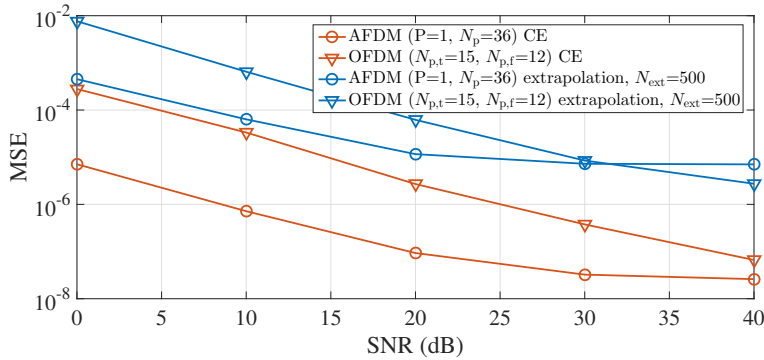


Fig. 11. MSE of Channel estimation and prediction for  $N = 2048, L = 20, Q = 7, p_d = 0.2, p_D = 0.2, N_s = 32, N_{\text{fft}}=64$

Figure 11 illustrates that, when dealing with off-grid Doppler shift values, AFDM maintains its superiority proved with the on-grid model. Indeed, the values of  $N_p$ ,  $N_{p,t}$  and  $N_{p,f}$  used to generate the figure, while yielding almost identical pilot overheads for OFDM and AFDM ( $\text{overhead}_{\text{AFDM}} = 767$ ,  $\text{overhead}_{\text{OFDM}} = 769$ , result in a superior MSE performance for AFDM in both channel estimation and channel prediction tasks.

## VI. CONCLUSIONS

This paper investigated channel estimation for doubly sparse LTV channels, addressing both on-grid and off-grid Doppler shifts. The on-grid approximation was used to provide rigorous recovery guarantees when channel estimation is done based on different underlying waveforms. To handle off-grid effects, we introduced a DPSS-based model consisting of multiple elementary BEMs and we provided analytical precision guarantees for that model. Additionally, a channel prediction method was proposed by taking advantage of DPSS extrapolation capability. Numerical results confirmed AFDM's superiority in both estimation and prediction under double (delay-Doppler) sparsity, making it a strong candidate for future wireless systems.

## APPENDIX A

### PROOF OF THEOREM 1

In the case of SCW, defining  $\tilde{\alpha}_{l,q} \triangleq \alpha_{l,q} e^{i2\pi \frac{lq}{N}}$ , rearranging  $\mathbf{y}_p$  into  $\tilde{\mathbf{y}}_p$  (composed of  $L$  successive blocks, with the  $l$ -th blocks composed of the  $l$ -th sample in each of the  $N_p$  pilot intervals) and assuming  $2Q + 1$  divides  $N$  and that the  $p$ -th pilot position (for any  $p \in \llbracket 1..N_p \rrbracket$ ) satisfies  $m_p = q_p \frac{N}{2Q+1}$  for some  $q_p \in \llbracket 0..2Q \rrbracket$ , we can write  $\tilde{\mathbf{y}}_p = \tilde{\mathbf{M}}_p^{\text{scw}} \tilde{\boldsymbol{\alpha}}$  where  $\tilde{\boldsymbol{\alpha}}$  is the

vectorized form of  $\tilde{\alpha}_{l,q}$  and  $\widetilde{\mathbf{M}}_p^{\text{scw}} \triangleq \mathbf{I}_L \otimes (\text{diag}(p_1, \dots, p_{N_p}) \overline{\mathbf{F}}_{2Q+1, N_p})$ . Here,  $\overline{\mathbf{F}}_{2Q+1, N_p}$  is the partial inverse Fourier measurement matrix formed from  $N_p$  rows of the  $(2Q+1)$ -point inverse DFT matrix. The HiRIP of  $\widetilde{\mathbf{M}}_p^{\text{scw}}$  can thus be derived and proven to be equal to the value given in the theorem statement by using the known RIP of partial inverse Fourier measurement matrices [28, Theorem 4.5] followed by applying [18, Theorem 4] pertaining to the HiRIP of hierarchical measurement matrices having the Kronecker property. This completes the part of the proof related to SCM.

As for OFDM, it can be shown that the estimation problem has a measurement matrix  $\widetilde{\mathbf{M}}_p^{\text{ofdm}} \triangleq (\text{diag}(p_1, \dots, p_{N_{p,f}}) \mathbf{F}_{L, N_{p,f}}) \otimes \overline{\mathbf{F}}_{2Q+1, N_{p,t}}$  where  $\mathbf{F}_{L, N_{p,f}}$  is the partial Fourier measurement matrix formed from  $N_{p,f}$  rows of the  $L$ -point inverse DFT matrix. The value of the HiRIP of  $\widetilde{\mathbf{M}}_p^{\text{ofdm}}$  given in the statement of the theorem thus follows from the RIP of the partial Fourier measurement matrix and the HiRIP result pertaining to Kronecker hierarchical measurements.

## APPENDIX B

### PROOF OF THEOREM 2

First, out of the pilot samples set  $\mathcal{P}$ , consider the subset  $\mathcal{P}_p$  associated with the  $p$ -th pilot symbol transmitted at the DAFT index  $m_p$  (Fig. 4). To homogenize the sensing signal model associated with edge samples and inner samples of  $\mathcal{P}_p$ , we apply two overlap-add operations: adding the samples received within the index interval  $\llbracket m_p - Q .. m_p - 1 \rrbracket$  to those received within  $\llbracket m_p + (L-1)P - Q .. m_p + (L-1)P - 1 \rrbracket$  and the samples received within  $\llbracket m_p + (L-1)P + 1 .. m_p + (L-1)P + Q \rrbracket$  to those received within  $\llbracket m_p + 1 .. m_p + Q \rrbracket$ . Now, define

$$\mathcal{D}_l \triangleq \left\{ (\tilde{l}, q) \text{ s.t. } (q + P\tilde{l})_{(L-1)P+1} = l \right\} \quad (43)$$

as the set of delay-Doppler grid points that potentially contribute to the pilot sample received at DAFT domain index  $l \in \llbracket m_p .. m_p + (L-1)P \rrbracket$  (Fig. 12) after the two overlap-add operations described above. Note that  $\mathcal{D}_l$  does not depend on the pilot symbol index  $p$  and that it has a cardinality that does not change with  $l$  and which satisfies  $|\mathcal{D}_l| \leq 2\lceil \frac{Q}{P} \rceil + 1$ . Next, define  $\boldsymbol{\alpha}_{\mathcal{D}_l} \triangleq [\alpha_{l,q}]_{(l,q) \in \mathcal{D}_l}$  and  $\tilde{\boldsymbol{\alpha}} \triangleq \left[ \boldsymbol{\alpha}_{\mathcal{D}_0}^T \quad \dots \quad \boldsymbol{\alpha}_{\mathcal{D}_{(L-1)P}}^T \right]^T$ . The entries of  $\tilde{\boldsymbol{\alpha}}$  are just a permutation of the entries of  $\boldsymbol{\alpha}$  and estimating one of these vectors directly gives an estimate of the other. Now, it can be shown that when we set  $P$  as in the theorem and  $\epsilon > 0$  as small as needed, then  $\tilde{\boldsymbol{\alpha}}$  is  $(\tilde{s}_d, \tilde{s}_D)$ -hierarchically sparse with high probability.

$$\tilde{s}_d = (L-1)P + 1, \quad \tilde{s}_D = (1 + \epsilon) \log(LP). \quad (44)$$



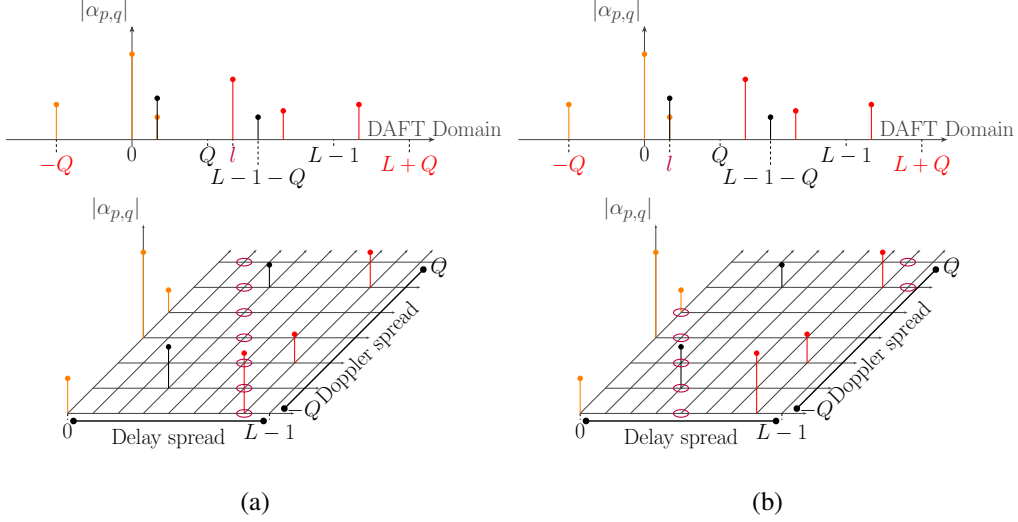


Fig. 12. Two examples of the set  $\mathcal{D}_l$  ( $P = 1, m_p = 0$ ) (a) for an  $l$  resulting in a whole diagonal, (b) for an  $l$  resulting in a wrapped diagonal. In each one of the two examples, the grid points forming  $\mathcal{D}_l$  are shown surrounded by red rings.

Indeed, the first level (of size  $(L-1)P+1$ ) of  $\tilde{\alpha}$  is sensed without compression with a number of measurements equal to  $(L-1)P+1$  while  $\tilde{s}_D$  can be determined thanks to Definition 1 and Assumptions 1 and 2 and applying the same approach as in the proof of Lemma 1 to  $\tilde{S}_{D,l} \triangleq \sum_{(\tilde{l},q) \in \mathcal{D}_l} I_{\tilde{l},q}$ . Now, we can write the signal model of sensing  $\tilde{\alpha}$  as

$$\tilde{\mathbf{y}}_p = \tilde{\mathbf{M}}_p \tilde{\alpha} + \tilde{\mathbf{w}}_p, \quad (45)$$

where  $\tilde{\mathbf{y}}_p = [\tilde{\mathbf{y}}_{p,0}^T \cdots \tilde{\mathbf{y}}_{p,(L-1)P}^T]^T$ . For each  $l$ ,  $\tilde{\mathbf{y}}_{p,l}$  is a  $N_p \times 1$  vector composed of the pilot samples received at DAFT domain positions  $\{m_p + l\}_{p=1 \dots N_p}$ . Note that by this definition  $\tilde{\mathbf{y}}_p$  is obtained by permuting  $\mathbf{y}_p$  in (29) in accordance with the permutation that gives  $\tilde{\alpha}$  from  $\alpha$ . Next, by setting for each  $p \in \llbracket 1 \dots N_p \rrbracket$   $m_p = q_p \frac{N}{2^{\lceil \frac{Q}{P} \rceil + 1}}$  for some integer  $q_p$  it follows from (14) and (43) that  $\tilde{\mathbf{M}}_p$  has the following Kronecker structure

$$\tilde{\mathbf{M}}_p = \mathbf{I}_{(L-1)P+1} \otimes \tilde{\mathbf{M}}_D, \quad (46)$$

with  $\tilde{\mathbf{M}}_D = \text{diag}(p_1 \cdots p_{N_p}) \mathbf{F}_{2^{\lceil \frac{Q}{P} \rceil + 1}, N_p} \mathbf{\Psi}$ ,  $\mathbf{F}_{2^{\lceil \frac{Q}{P} \rceil + 1}, N_p}$  is a  $(2^{\lceil \frac{Q}{P} \rceil + 1}) \times N_p$  partial Fourier measurement matrix and  $\mathbf{\Psi}$  is a diagonal matrix with unit-modulus entries. We can thus use [28, Theorem 4.5] pertaining to sub-sampled Fourier matrices to get that for sufficiently large  $L, Q$ , sufficiently small  $\delta$ , and

$$N_p > O\left(\frac{1}{\delta^2} \log^2 \frac{1}{\delta} \log \frac{\log(LP)}{\delta} \log(LP) \log \frac{Q}{P}\right) \quad (47)$$

the RIP constant  $\delta_{\tilde{\mathbf{M}}_D}$  of  $\tilde{\mathbf{M}}_D$  satisfies  $\delta_{\tilde{\mathbf{M}}_D} \leq \delta$  with probability  $1 - e^{-\Omega(\log \frac{Q}{P} \log \frac{1}{\delta})}$ . The RIP of  $\mathbf{I}_{(L-1)P+1}$  trivially satisfies  $\delta_{\tilde{\mathbf{s}}_d} = 0$ . As for the HiRIP of  $\tilde{\mathbf{M}}_p$ , we can apply [18, Theorem 4] to (46) thanks to its Kronecker structure to get that, f  $N_p$  and  $\delta$  are as in (47), then

$$\delta_{s_d, s_D} \leq \delta_{\tilde{\mathbf{s}}_d} + \delta_{\tilde{\mathbf{s}}_D} + \delta_{\tilde{\mathbf{s}}_d} \delta_{\tilde{\mathbf{s}}_D} \leq \delta. \quad (48)$$

This completes the proof of the theorem.

## APPENDIX C

### PROOF OF THEOREM 3

We first need the following lemma taken from [29, Theorem 2.4].

**Lemma 2.** [29, Theorem 2.4] *Let  $h(t)$  be a continuous-time zero-mean wide-sense stationary random process with power spectrum  $P_h(f) = \frac{1}{B} \text{rect}(\frac{f-F_c}{2B})$ . Denote by  $\mathbf{h} = [h(0T_s) \dots h((N-1)T_s)]^T$  a vector of samples acquired from  $h(t)$  with a sampling period  $T_s \leq \frac{1}{2F_c+B}$ . Let  $W = \frac{BT_s}{2}$ ,  $\mathbf{U}_k$  the matrix form of the  $k$  first  $(N, W)$ -DPSS vectors,  $\mathbf{E}_f \triangleq \text{diag}(e^{i2\pi f_0} \dots e^{i2\pi f(N-1)})$  and  $\mathbf{P}_k \triangleq \mathbf{E}_{F_c T_s} \mathbf{U}_k \mathbf{U}_k^H \mathbf{E}_{F_c T_s}^H$ . Then  $\mathbb{E}[\|\mathbf{h} - \mathbf{P}_k \mathbf{h}\|_2^2] = \frac{1}{2W} \sum_{l=k}^{N-1} \lambda_l^{(N, W)}$ .*

In what follows, we use Lemma 2 to upper bound  $\mathbb{E}[|h_{l,q,n} - h_{l,q,n}^{\text{BEM}}|^2]$ . For that sake, we rewrite  $h_{l,q,n}$  as the sampled version of the continuous-time signal  $h_{l,q}(t)$  defined as

$$h_{l,q}(t) \triangleq \sum_{i=1}^{N_D} \alpha_{l,q,i} e^{i2\pi f_i t}, \quad t \in \mathbb{R}. \quad (49)$$

with  $f_i \triangleq \frac{q}{NT_s} + \frac{\kappa_i}{NT_s}$ . To prove that the PSD of the random process  $h_{l,q}(t)$  has the desired property, we derive its autocorrelation function  $R_{h_{l,q}}(\tau) \triangleq \mathbb{E}[h_{l,q}(t)h_{l,q}^*(t+\tau)]$  as

$$\begin{aligned} R_{h_{l,q}}(\tau) &= \sum_{i=1}^{N_D} \sum_{j=1}^{N_D} \mathbb{E}[\alpha_{l,q,i} \alpha_{l,q,j}^*] \mathbb{E}[e^{i2\pi f_i t} e^{-i2\pi f_j (t+\tau)}] \\ &= \sum_{i=0}^{N_D} \sigma_\alpha^2 \mathbb{E}[e^{-i2\pi f_i \tau}] \end{aligned} \quad (50)$$

where the first equality is due to (49) and the second to  $f_i \sim \mathcal{U}\left(\left[\frac{q}{NT_s} - \frac{1}{2NT_s}, \frac{q}{NT_s} + \frac{1}{2NT_s}\right]\right)$ ,  $\alpha_{l,q,i} \sim \mathcal{CN}(0, \sigma_\alpha^2)$  and the independence property of  $\{\alpha_{l,q,i}\}_i$  as per Definition 4. This gives:

$$R_{h_{l,q}}(\tau) = N_D \sigma_\alpha^2 e^{-i2\pi \frac{q}{NT_s} \tau} \text{sinc}\left(\frac{\tau}{NT_s}\right). \quad (51)$$

The power spectral density (PSD) is thus

$$P_{h_{l,q}}(f) \triangleq \mathcal{F}\{R_{h_{l,q}}(\tau)\} = N_D \sigma_\alpha^2 NT_s \text{rect}\left(\left(f - \frac{q}{NT_s}\right) NT_s\right). \quad (52)$$

The PSD of  $h_{l,q}(t)$  thus satisfies the condition of Lemma 2 with  $B = \frac{1}{2NT_s}$  and  $F_c = \frac{q}{NT_s}$  giving

$$\mathbb{E} \left[ |h_{l,q,n} - h_{l,q,n}^{\text{BEM}}|^2 \right] = \frac{1}{N} \mathbb{E} \left[ \|\mathbf{h}_{l,q} - \mathbf{h}_{l,q}^{\text{BEM}}\|^2 \right] = \frac{N_D \sigma_\alpha^2}{2WN} \sum_{b=Q_{\text{BEM}}}^{N-1} \lambda_b^{(N,W)}. \quad (53)$$

Now define  $\lambda_b^{(c)}$  as the  $b$ -th eigenvalue of the prolate spheroidal wave functions (PSWF) [30] with the bandwidth parameter  $c \triangleq \pi NW$ . This allows us to exploit existing results on the behavior of PSWF eigenvalues in the limit of  $c \rightarrow \frac{\pi}{2}$  (or equivalently as  $W$  tends to zero at the rate  $\frac{1}{2N}$ ) to upper bound the sum of DPSS eigenvalues  $\lambda_b^{(N,W)}$  in (53). Indeed, due to [31, Theorem 2]

$$\lambda_b^{(N,W)} \leq A_W \lambda_b^{(c)}, \forall b = 1, \dots, N. \quad (54)$$

Here,  $A_W$  is a function of  $W$  defined in [31, Eq. (45)] and whose image is fully included in the interval  $\left[\frac{\pi^2}{8}, 2\right]$ . Plugging (54) into (53) and noting that  $2WN = 1$  lead to

$$\mathbb{E} \left[ |h_{l,q,n} - h_{l,q,n}^{\text{BEM}}|^2 \right] \leq N_D \sigma_\alpha^2 A_W \sum_{b=Q_{\text{BEM}}}^N \lambda_b^{(c)} \quad (55)$$

The right-hand side term in (55) can be upper bounded due to the fact that the PSWF eigenvalues decay at least exponentially<sup>1</sup> as  $b$  grows beyond  $\frac{2\pi NW}{\pi} + O(\log(\pi NW)) = 1 + O(\log \frac{\pi}{2})$ . More precisely, it follows from [33, Theorem 2.5] that  $\lambda_b^{(c)} = O\left(e^{-\frac{\pi}{\log \frac{\pi}{2}} b}\right)$ . Plugging this into (55) results, for any  $\epsilon > 0$  and  $Q_{\text{BEM}} > C \log \frac{2}{\epsilon}$  for sufficiently large  $C$ , in

$$\mathbb{E} \left[ |h_{l,q,n} - h_{l,q,n}^{\text{BEM}}|^2 \right] < \frac{N_D \sigma_\alpha^2 A_W \epsilon}{2}. \quad (56)$$

Now, note that

$$\begin{aligned} \mathbb{E} \left[ \sum_{l=0}^{L-1} |h_{l,n} - h_{l,n}^{\text{BEM}}|^2 \right] &= \mathbb{E} \left[ \sum_{l=0}^{L-1} \left| \sum_{q=-Q}^Q I_{l,q} e^{i2\pi \frac{nq}{N}} \sum_{b=1}^{Q_{\text{BEM}}} (h_{l,q,n} - h_{l,q,n}^{\text{BEM}}) \right|^2 \right] \\ &= \sum_{l=0}^{L-1} \sum_{q=-Q}^Q \mathbb{E} [I_{l,q}] \mathbb{E} \left[ |h_{l,q,n} - h_{l,q,n}^{\text{BEM}}|^2 \right] \end{aligned} \quad (57)$$

Plugging (56) into the right-hand side of (57) gives

$$\mathbb{E} \left[ \sum_{l=0}^{L-1} |h_{l,n} - h_{l,n}^{\text{BEM}}|^2 \right] < \sum_{l=0}^{L-1} \sum_{q=-Q}^Q \mathbb{E} [I_{l,q}] \frac{N_D \sigma_\alpha^2 A_W \epsilon}{2} \leq \epsilon \quad (58)$$

where the second inequality is due to the fact that  $A_W \leq 2$  and that  $\sum_{l=0}^{L-1} \sum_{q=-Q}^Q \mathbb{E} [I_{l,q}] = \frac{1}{N_D \sigma_\alpha^2}$  due to the power normalization condition in (18). This completes the proof of the theorem.

<sup>1</sup>Actually, even super-geometric decay can be proven [32]

## APPENDIX D

## PROOF OF THEOREM 4

In what follows we use the notation  $h_{l,q,n}^{\text{ext}} \left( \hat{\mathbf{h}}_{l,q}^{\text{BEM}} \right)$  to designate the DPSS extrapolation predictor defined in (37) to highlight its dependence on the estimated vector  $\hat{\mathbf{h}}_{l,q}^{\text{BEM}}$ . When  $\hat{\mathbf{h}}_{l,q}^{\text{BEM}}$  in (37) is replaced with an arbitrary channel vector  $\mathbf{h}$ , the DPSS predictor generalizes to

$$h_{l,q,n}^{\text{ext}}(\mathbf{h}) \triangleq \underbrace{e^{i2\pi \frac{nq}{N}} \left( \mathbf{u}_n^{\text{ext}} \right)^{\text{T}} \mathbf{U}_{Q_{\text{BEM}}}^{\text{H}} \mathbf{E}_{\frac{q}{N}}^{\text{H}} \mathbf{h}}_{\triangleq \left( \mathbf{f}_{Q_{\text{BEM}}}^{\text{ext}} \right)^{\text{H}}} \quad (59)$$

For instance,  $h_{l,q,n}^{\text{ext}} \left( \mathbf{h}_{l,q}^{\text{BEM}} \right)$  is the DPSS predictor based on the actual, not the estimated, vector  $\mathbf{h}_{l,q}^{\text{BEM}}$ . Next, we establish the link between the DPSS extrapolation predictor and MMSE prediction given the knowledge of the channel during the observation interval.

For that sake first note that for each  $l, q$  and any  $n \in \mathbb{Z}$ , the random variable  $h_{l,q,n}$  as defined by (22) follows a complex symmetric Gaussian distribution  $\mathcal{CN}(0, N_{\text{D}}\sigma_{\alpha}^2)$  under the conditions of Definition 4. Moreover, the random process  $(h_{l,q,n})_{n \in \mathbb{Z}}$  is stationary and has an auto-correlation  $\mathbb{E} [h_{l,q,n} h_{l,q,m}^*] = \sigma_{\alpha}^2 N_{\text{D}} e^{i2\pi \frac{(n-m)q}{N}} \frac{N}{\pi(n-m)} \sin \left( \frac{\pi(n-m)}{N} \right)$  due to (22). Similarly,  $\mathbf{h}_{l,q} \sim \mathcal{CN} \left( \mathbf{0}, \sigma_{\alpha}^2 N_{\text{D}} N \mathbf{E}_{\frac{q}{N}} \boldsymbol{\Sigma} \mathbf{E}_{\frac{q}{N}}^{\text{H}} \right)$  and  $\mathbf{h}_{l,q}^{\text{BEM}} \sim \mathcal{CN} \left( \mathbf{0}, \sigma_{\alpha}^2 N_{\text{D}} N \mathbf{E}_{\frac{q}{N}} \mathbf{P}^{\text{BEM}} \boldsymbol{\Sigma} \mathbf{P}^{\text{BEM}} \mathbf{E}_{\frac{q}{N}}^{\text{H}} \right)$  with

$$\boldsymbol{\Sigma} \triangleq \left[ \frac{1}{\pi(n-m)} \sin \frac{\pi(n-m)}{N} \right]_{\substack{n=0 \dots N-1 \\ m=0 \dots N-1}} = [C_{n,m}^{(N,W)}]_{\substack{n=0 \dots N-1 \\ m=0 \dots N-1}} \quad (60)$$

Therefore, the MMSE predictor of  $h_{l,q,n}$  given the actual channel component  $\mathbf{h}_{l,q}$  is

$$\begin{aligned} \hat{h}_{l,q,n}(\mathbf{h}_{l,q}) &= \mathbf{E} [h_{l,q,n} \mathbf{h}_{l,q}^{\text{H}}] \left( \mathbf{E} [\mathbf{h}_{l,q} \mathbf{h}_{l,q}^{\text{H}}] \right)^{-1} \mathbf{h}_{l,q} \\ &= e^{i2\pi \frac{nq}{N}} \boldsymbol{\rho} \mathbf{E}_{\frac{q}{N}} \boldsymbol{\Sigma}^{-1} \mathbf{E}_{\frac{q}{N}}^{\text{H}} \mathbf{h}_{l,q}. \end{aligned} \quad (61)$$

Here  $\boldsymbol{\rho} \triangleq \left[ e^{-i2\pi \frac{mq}{N}} C_{n,m}^{(N,W)} \right]_{m=0}^{N-1}$ . It follows that the reduced-rank MMSE predictor  $\hat{h}_{l,q,n}^{\text{RR}}$  of rank  $Q$  of  $h_{l,q,n}$  given  $\mathbf{h}_{l,q}$  (where notation ‘RR’ stands for ‘reduced rank’) is [34]

$$\hat{h}_{l,q,n}^{\text{RR}}(\mathbf{h}_{l,q}) = \left( \mathbf{f}_Q^{\text{RR}} \right)^{\text{H}} \mathbf{h}_{l,q}, \quad (62)$$

$$\mathbf{f}_Q^{\text{RR}} \triangleq \mathbf{E}_{\frac{q}{N}} \mathbf{U}_Q \text{diag} \left( \frac{1}{\lambda_1^{(N,W)}}, \dots, \frac{1}{\lambda_Q^{(N,W)}} \right) \mathbf{U}_Q^{\text{H}} \mathbf{E}_{\frac{q}{N}}^{\text{H}} \boldsymbol{\rho}^{\text{H}}. \quad (63)$$

Next, we apply the triangle inequality to get

$$\begin{aligned} \mathbb{E} \left[ \left| h_{l,q,n}^{\text{ext}} \left( \hat{\mathbf{h}}_{l,q}^{\text{BEM}} \right) - \hat{h}_{l,q,n}^{\text{RR}}(\mathbf{h}_{l,q}) \right|^2 \right] &\leq \underbrace{\mathbb{E} \left[ \left| h_{l,q,n}^{\text{ext}} \left( \hat{\mathbf{h}}_{l,q}^{\text{BEM}} \right) - h_{l,q,n}^{\text{ext}} \left( \mathbf{h}_{l,q}^{\text{BEM}} \right) \right|^2 \right]}_{\triangleq E_1} + \\ &\underbrace{\mathbb{E} \left[ \left| h_{l,q,n}^{\text{ext}} \left( \mathbf{h}_{l,q}^{\text{BEM}} \right) - h_{l,q,n}^{\text{ext}}(\mathbf{h}_{l,q}) \right|^2 \right]}_{\triangleq E_2} + \underbrace{\mathbb{E} \left[ \left| h_{l,q,n}^{\text{ext}}(\mathbf{h}_{l,q}) - \hat{h}_{l,q,n}^{\text{RR}}(\mathbf{h}_{l,q}) \right|^2 \right]}_{\triangleq E_3}. \end{aligned} \quad (64)$$

Since  $\lim_{\sigma_w^2 \rightarrow 0} \mathbb{E} \left[ \left\| \hat{\mathbf{h}}_{l,q}^{\text{BEM}} - \mathbf{h}_{l,q}^{\text{BEM}} \right\|^2 \right]$  due to Assumption 3, it follows from (59) by standard MSE derivations that  $\lim_{\sigma_w^2 \rightarrow 0} E_1 = 0$ . As for  $E_2$ , and since  $\mathbf{h}_{l,q}^{\text{BEM}} = \mathbf{E}_{\frac{q}{N}} \mathbf{P}^{\text{BEM}} \mathbf{E}_{\frac{q}{N}}^H \mathbf{h}_{l,q}$  per (25), we have that  $\mathbf{U}_{Q_{\text{BEM}}}^H \mathbf{E}_{\frac{q}{N}}^H \mathbf{h}_{l,q} = \mathbf{U}_{Q_{\text{BEM}}}^H \mathbf{E}_{\frac{q}{N}}^H \mathbf{h}_{l,q}^{\text{BEM}}$ . It follows from (59) that  $h_{l,q,n}^{\text{ext}}(\mathbf{h}_{l,q}) = h_{l,q,n}^{\text{ext}}(\mathbf{h}_{l,q}^{\text{BEM}})$  and hence that  $E_2 = 0$ . Finally, note by referring to (35), (59) and (63) that  $\mathbf{f}_Q^{\text{RR}} = \mathbf{f}_{Q_{\text{BEM}}}^{\text{ext}}$  if  $Q = Q_{\text{BEM}}$  leading to  $E_3 = 0$ .

Now, due to (35),  $h_{l,n}^{\text{ext}} = \sum_{l=0}^{L-1} I_{l,q} h_{l,q,n}^{\text{ext}}$ . Moreover, due to the independence conditions from Definition 4,  $\hat{h}_{l,n}^{\text{RR}} \triangleq \sum_{l=0}^{L-1} I_{l,q} \hat{h}_{l,q,n}^{\text{RR}}$  is the reduced-rank MMSE estimate of  $h_{l,n}$  given  $\{\mathbf{h}_{l,q}\}_{q=-Q \dots Q}$  and conditioned on a given realization of  $I_{l,q}$ . Putting all these pieces together, it follows that  $\lim_{\sigma_w^2 \rightarrow 0} \left| h_{l,n}^{\text{ext}} - \hat{h}_{l,n}^{\text{RR}} \right|^2$ . This completes the proof of the theorem.

## REFERENCES

- [1] A. J. G. F. Gómez-Cuba, “Compressed sensing channel estimation for OFDM with non-Gaussian multipath gains,” *IEEE Trans. Wireless Commun.*, vol. 19, no. 1, pp. 47–61, 2020.
- [2] C. R. Berger, Z. Wang, J. Huang, and S. Zhou, “Application of compressive sensing to sparse channel estimation,” *IEEE Communications Magazine*, vol. 48, no. 11, pp. 164–174, 2010.
- [3] C. K. Thomas and D. Slock, “BP-VB-EP based static and dynamic sparse Bayesian learning with kronecker structured dictionaries,” in *IEEE ICASSP*, 2020, pp. 9095–9099.
- [4] G. Tauböck and F. Hlawatsch, “A compressed sensing technique for OFDM channel estimation in mobile environments: Exploiting channel sparsity for reducing pilots,” in *ICASSP*, 2008, pp. 2885–2888.
- [5] Y. Chi, L. L. Scharf, A. Pezeshki, and A. R. Calderbank, “Sensitivity to basis mismatch in compressed sensing,” *IEEE Trans. on Signal Processing*, vol. 59, no. 5, pp. 2182–2195, 2011.
- [6] S. Ganguly, I. Ghosh, R. Ranjan, J. Ghosh, P. K. Kumar, and M. Mukhopadhyay, “Compressive sensing based off-grid doa estimation using omp algorithm,” in *SPIN*, 2019, pp. 772–775.
- [7] C. Tian, J. Zhang, Q. Meng, and D. Wang, “Microwave staring correlated imaging using BOMP based on adaptive meshing,” *2016 CIE International Conference on Radar (RADAR)*, pp. 1–4, 2016.
- [8] R. Beinert, P. Jung, G. Steidl, and T. Szollmann, “Super-resolution for doubly-dispersive channel estimation,” 2021.
- [9] H. Groll *et al.*, “Sparsity in the delay-Doppler domain for measured 60 GHz vehicle-to-infrastructure communication channels,” in *IEEE ICC Workshops*, 2019.
- [10] Z. Lu, R. Ying, S. Jiang, Z. Zhang, P. Liu, and W. Yu, “Distributed compressed sensing off the grid,” *IEEE Signal Processing Letters*, vol. 22, 07 2014.
- [11] A. Mohebbi, H. Abdzadeh-Ziabari, W.-P. Zhu, and M. O. Ahmad, “Doubly selective channel estimation algorithms for millimeter wave hybrid MIMO systems,” *IEEE Trans. on Veh. Technol.*, vol. 70, no. 12, pp. 12 821–12 835, 2021.
- [12] D. Fu, Y. Peng, and S. Zheng, “A compressive channel sensing method with optimal thresholding for OFDM systems under fast fading channels,” in *2016 IEEE Wireless Communications and Networking Conference*, 2016, pp. 1–5.
- [13] Y. Liu, Y. L. Guan, and D. G. G., “Near-optimal BEM OTFS receiver with low pilot overhead for high-mobility communications,” *IEEE Trans. Commun.*, vol. 70, no. 5, pp. 3392–3406, 2022.
- [14] L. Gaudio, G. Colavolpe, and G. Caire, “OTFS vs. OFDM in the presence of sparsity: A fair comparison,” *IEEE Trans. Wireless Commun.*, vol. 21, no. 6, pp. 4410–4423, 2022.

- [15] A. Bemani, N. Ksairi, and M. Kountouris, "Affine frequency division multiplexing for next generation wireless communications," *IEEE Transactions on Wireless Communications*, vol. 22, no. 11, pp. 8214–8229, 2023.
- [16] W. Benzine, A. Bemani, N. Ksairi, and D. Slock, "Affine frequency division multiplexing for communications on sparse time-varying channels," in *IEEE GLOBECOM*, 2023, pp. 4921–4926.
- [17] —, "Affine frequency division multiplexing for compressed sensing of time-varying channels," in *2024 IEEE 25th International Workshop on Signal Processing Advances in Wireless Communications (SPAWC)*, 2024, pp. 916–920.
- [18] I. Roth, M. Kliesch, A. Flinth, G. Wunder, and J. Eisert, "Reliable recovery of hierarchically sparse signals for Gaussian and Kronecker product measurements," *IEEE Trans. Signal Process.*, vol. 68, pp. 4002–4016, 2020.
- [19] H. Shayanfar, W.-P. Zhu, and M. Swamy, "Compressed sensing based channel estimation for GFDM systems in high mobility scenario," in *IEEE SPAWC*, 2023, pp. 266–270.
- [20] W. Li, H. Yin, Z. Qin, Y. Cao, and M. Debbah, "A multi-dimensional matrix pencil-based channel prediction method for massive MIMO with mobility," *IEEE Trans. on Wireless Communications*, vol. 22, no. 4, pp. 2215–2230, 2023.
- [21] S. Uehashi, Y. Ogawa, T. Nishimura, and T. Ohgane, "Prediction of time-varying multi-user MIMO channels based on DoA estimation using compressed sensing," *IEEE Trans. on Veh. Technol.*, vol. 68, no. 1, pp. 565–577, 2019.
- [22] P. Chaki, J. Shikida, and K. Muraoka, "Exploiting sparse matrix solution to mitigate channel aging in sub-6 GHz 5G MU-MIMO using beamspace-delay-doppler domain," in *IEEE ICC*, 2024, pp. 475–480.
- [23] T. Zemen, C. Mecklenbrauker, F. Kaltenberger, and B. Fleury, "Minimum-energy band-limited predictor with dynamic subspace selection for time-variant flat-fading channels," *IEEE Trans. on Signal Processing*, vol. 55, no. 9, pp. 4534–4548, 2007.
- [24] S. Karnik, Z. Zhu, M. B. Wakin, J. Romberg, and M. A. Davenport, "The fast slepian transform," *Applied and Computational Harmonic Analysis*, vol. 46, no. 3, pp. 624–652, 2019.
- [25] P. Cheng, Z. Chen, Y. Rui, Y. J. Guo, L. Gui, M. Tao, and Q. T. Zhang, "Channel estimation for OFDM systems over doubly selective channels: A distributed compressive sensing based approach," *IEEE Transactions on Communications*, vol. 61, no. 10, pp. 4173–4185, 2013.
- [26] D. Thomson, "Spectrum estimation and harmonic analysis," *Proceedings of the IEEE*, vol. 70, no. 9, pp. 1055–1096, 1982.
- [27] S. Kay, *Fundamentals of Statistical Signal Processing: Estimation theory*. Prentice-Hall PTR, 2013.
- [28] I. Haviv and O. Regev, "The restricted isometry property of subsampled Fourier matrices," in *Geometric Aspects of Functional Analysis: Israel Seminar (GAFA) 2014–2016*. Springer, 2017, pp. 163–179.
- [29] Z. Zhu and M. B. Wakin, "Approximating sampled sinusoids and multiband signals using multiband modulated DPSS dictionaries," *Journal of Fourier Analysis and Applications*, vol. 23, no. 6, pp. 1531–5851, December 2017.
- [30] D. Slepian, "Prolate spheroidal wave functions, fourier analysis, and uncertainty — v: The discrete case," *The Bell System Technical Journal*, vol. 57, no. 5, pp. 1371–1430, 1978.
- [31] M. Bouslane, N. Bourguiba, and A. Karoui, "Discrete prolate spheroidal wave functions: Further spectral analysis and some related applications," *Journal of Scientific Computing*, vol. 82, no. 3, February 2020.
- [32] L.-L. WANG, "Analysis of spectral approximations using prolate spheroidal wave functions," *Mathematics of Computation*, vol. 79, no. 270, pp. 807–827, 2010.
- [33] H. Xiao, V. Rokhlin, and N. Yarvin, "Prolate spheroidal wavefunctions, quadrature and interpolation," *Inverse Problems*, vol. 17, no. 4, p. 805, August 2001.
- [34] F. Rubio and X. Mestre, "Consistent reduced-rank LMMSE estimation with a limited number of samples per observation dimension," *IEEE Trans. on Signal Processing*, vol. 57, no. 8, pp. 2889–2902, 2009.